



Phytoplankton primary productivity: A dual-incubation approach for direct comparison of photosystem II photosynthetic flux (JV_{PII}) and ^{14}C -fixation experiments

Nina Schuback ^{1,2,*}, Kevin Oxborough,^{1,3} Mary Burkitt-Gray ^{1,a}, Patricia López-García,⁴ Matthew D. Patey,⁴ Emily Hammermeister,⁴ Alan Wright,^{3,b} C. Mark Moore^{3*}

¹Chelsea Technologies Ltd., West Molesey, UK

²Swiss Polar Institute, Sion, Switzerland

³School of Ocean and Earth Science, National Oceanography Centre Southampton, University of Southampton, Southampton, UK

⁴National Oceanography Centre, Southampton, UK

Abstract

Singe-turnover active chlorophyll *a* fluorometry (STAF) can be used to assess phytoplankton photosynthetic rates in terms of the photosystem II photochemical flux (JV_{PII} , $\mu\text{mol e}^- \text{m}^{-3} \text{s}^{-1}$) instantaneously, autonomously, and at high resolution. While JV_{PII} provides an upper limit to rates of phytoplankton primary productivity in units of carbon fixation, the conversion between these two rates is variable, limiting our ability to utilize high-resolution JV_{PII} data to monitor phytoplankton primary productivity. Simultaneous measurements of JV_{PII} and ^{14}C -fixation help in understanding the factors controlling the variable ratio between the two rates. However, to date, methodological inconsistencies, including differences in incubation lengths and light quality, have greatly inhibited practical assessment of such electron to carbon ratios ($\Phi_{e,C}$, $\text{mol e}^- \text{mol C}^{-1}$). We here present data from a range of dual-incubation experiments in northeast Atlantic waters during which JV_{PII} and ^{14}C -fixation were measured simultaneously on the same sample. Time-course experiments show how $\Phi_{e,C}$ increases with incubation length, likely reflecting the transition from gross to net ^{14}C -fixation. Dual-incubation experiments conducted under different light levels show a tendency for increased $\Phi_{e,C}$ under (super-)saturating light. Finally, data from a diurnal experiment demonstrate how $\Phi_{e,C}$ increases over the course of a day, due to downregulation of ^{14}C -fixation. We provide a detailed description of our methodological approach, including a critical discussion of improvements to the calculation of JV_{PII} implemented in the LabSTAF instrument used for active fluorescence measurements and the limitations of the well-established ^{14}C -fixation approach.

Primary production, the photosynthetic conversion of inorganic carbon into organic carbon products by marine phytoplankton, is one of the largest components of the global carbon cycle. It provides the basis of marine food webs and ecosystem dynamics and plays a pivotal role in regional and global

*Correspondence: schuback.nina@gmail.com, C.M.Moore@soton.ac.uk

Additional Supporting Information may be found in the online version of this article.

This is an open access article under the terms of the [Creative Commons Attribution-NonCommercial](https://creativecommons.org/licenses/by-nc/4.0/) License, which permits use, distribution and reproduction in any medium, provided the original work is properly cited and is not used for commercial purposes.

^aPresent address: Applied Ocean Physics & Engineering Department, Woods Hole Oceanographic Institution, Woods Hole, Massachusetts, USA

^bPresent address: University College London, London, UK

biogeochemical cycles and climate (Behrenfeld and Falkowski 1997; Kulk et al. 2020). Anthropogenic climate change is rapidly altering physical and chemical conditions in the global oceans which, in turn, will undoubtedly affect phytoplankton photosynthesis and primary production (Behrenfeld et al. 2006; Doney et al. 2012; Kulk et al. 2020). Our ability to monitor and model phytoplankton photosynthesis and primary production on meaningful temporal and spatial scales is therefore critical to track such changes and develop an understanding of potential feedback mechanisms to the global carbon cycle and climate (IPCC 2019). Despite this recognized importance it remains difficult to measure phytoplankton photosynthesis and primary productivity in situ at the sampling frequency, spatial coverage, and methodological consistency required to capture the spatio-temporal variability in this highly dynamic process.

Rates of photosynthesis and primary production can rapidly adjust to changes in the phytoplankton's integrated

growth environment including light, temperature, and nutrients (Behrenfeld et al. 2008). The changes in photosynthetic rates reflect the evolved optimization of the molecular process of photosynthesis on the physiological level as well as trait-based competitive changes in species composition. To understand and model changes in phytoplankton photosynthesis and primary production, rate measurements would ideally be obtained in situ and at a temporal resolution comparable to the rate of change in key abiotic drivers. While high-resolution autonomous in situ data for such physical and chemical parameters are increasingly available (Bax et al. 2019; Lombard et al. 2019), additional tools are required to monitor their effect on phytoplankton physiology and primary productivity.

Numerical modeling and satellite remote sensing are important tools for the monitoring of phytoplankton primary productivity on the global scale and are necessary to evaluate the response to climate change (Kulk et al. 2020; Westberry et al. 2023). Importantly, these approaches critically rely on a mechanistic understanding of how the entire photosynthetic process is controlled by environmental drivers and on the existence of large datasets of methodologically consistent in situ measurements covering all oceanic regions (Lee et al. 2015a; Li et al. 2022; Brewin et al. 2023).

Many methods are available to assess rates of phytoplankton primary production (International Ocean-Colour Coordinating Group [IOCCG] 2022). Arguably, the most direct approach to measure the fixation of inorganic carbon into organic matter is the use of the radioactive tracer ^{14}C (Steemann-Nielsen 1952). Compilations of ^{14}C -fixation experiments are used for the development and validation of remote sensing algorithms and the method is often regarded as the “gold-standard” against which other approaches are evaluated (IOCCG 2022). However, the method has a number of recognized limitations (Peterson 1980; Williams et al. 2002). For example, sample containment in incubation bottles for prolonged amounts of time can lead to changes in rate-determining physical (light, temperature) and chemical (nutrients) properties, relative to in situ conditions. Furthermore, the choice of incubation length, as well as the growth rate of the sampled phytoplankton, affect whether gross (all carbon fixed through photosynthesis) or net (carbon fixed after loss through autotrophic respiration) carbon fixation is estimated (Milligan et al. 2014; Halsey and Jones 2015). In addition, as samples are generally filtered after ^{14}C -fixation incubations, an unknown and variable fraction of primary productivity is always lost as dissolved organic carbon (DOC) (Viviani et al. 2015; Moran et al. 2022). Ultimately, ^{14}C -fixation approaches are not well suited for the collection of phytoplankton primary productivity data at the temporal and spatial resolution and methodological consistency required for the development of models and remote sensing approaches.

Single-turnover active fluorometry (STAF) is unique in providing autonomous, instantaneous, non-destructive, and sensitive observations of phytoplankton photosynthetic physiology

(Kolber and Falkowski 1993; Schuback et al. 2021). The method can be used to estimate rates of charge separation in photosystem II (referred to as electron transport rates, ETR_{PSII} , or photochemical flux, JV_{PII}). This rate quantifies the conversion of light energy into biochemical energy available for cellular metabolism including the fixation of inorganic carbon into organic matter, alongside other processes (Hughes et al. 2018b). Photosystem II photochemical flux thus provides an upper limit to rates of productivity in carbon units and is most closely linked to gross carbon fixation. A decoupling of JV_{PII} and gross carbon fixation reflects metabolic shifts in the allocation of photosynthetic energy away from carbon fixation at the physiological level and species succession at the community composition level (Hughes et al. 2018b, 2021; Schuback and Tortell 2019).

Many studies have sought to compare STAF derived rates of JV_{PII} with ^{14}C -fixation experiments, with the aim of characterizing the derived conversion factor $\Phi_{\text{e,C}}$ ($\text{e}^- \text{C}^{-1}$, the ratio of charge separations in PSII to carbon fixed) sufficiently well to utilize high-resolution STAF measurements for the assessment of phytoplankton primary productivity in carbon units (Lawrenz et al. 2013; Hughes et al. 2018b). A meta-analysis of these studies presented by Lawrenz et al. (2013) showed strong variability in $\Phi_{\text{e,C}}$ with observed values ranging from 1.2 to 54.2 $\text{mol e}^- \text{mol C}^{-1}$. However, studies comparing STAF with ^{14}C -fixation consistently highlight that it is often impossible to distinguish true physiological decoupling of the two rates from methodological artifacts caused by the use of parallel incubations, including differences in incubation lengths and spectral quality of light sources used (Lawrenz et al. 2013; Hughes et al. 2018b).

Methodological inconsistencies have thus likely reduced the accuracy of practical assessments of true electron to carbon ratios. Building on previous work by Suggett et al. (2009) and Hughes et al. (2020), we suggest a “dual-incubation” approach whereby both rates are measured simultaneously on the same sample. In the present study we present results from such dual-incubation experiments performed using LabSTAF instruments (Chelsea Technologies Ltd., CTL) using natural phytoplankton communities from the North Atlantic Ocean. Our aim is to provide methodological guidance, including a description of improved corrections applied within the derivation of JV_{PII} from STAF measurements, alongside more robust estimates of $\Phi_{\text{e,C}}$ within the system studied.

Data are presented from three sets of experiments: First, time-course experiments show how $\Phi_{\text{e,C}}$ increases with incubation length as a result of a decrease in measured ^{14}C -fixation rates. Second, 17 dual-incubations, conducted at limiting and saturating light, demonstrate a tendency for increased $\Phi_{\text{e,C}}$ under (super-)saturating light intensities, when compared to incubations performed under light limited conditions. Finally, data from a diurnal set of dual-incubation experiments show how $\Phi_{\text{e,C}}$ increases over the course of a day, due to down-regulation of ^{14}C -fixation.

The overall observed variability in $\Phi_{\text{e,C}}$ (3.0–12.1 $\text{e}^- \text{C}^{-1}$, mean 7.0 $\text{e}^- \text{C}^{-1}$, $n = 60$) is lower than many previous

observations. Some of this reduced variability can be attributed to the improved experimental approach. However, the proof-of-concept dataset presented here is small and only includes samples collected from nutrient replete waters within a limited temporal and geographical range and hence also across a limited range of community structures. Nevertheless, we hope that the described approach can provide a road-map for the collection of large and methodologically consistent datasets of $\Phi_{e,C}$ and caution that the interpretation of observed $\Phi_{e,C}$ values needs to include a critical assessment of what metabolic processes are being measured within ^{14}C -fixation experiments.

Materials and procedures

All data were collected during the research cruise DY149 on board the RRS Discovery, 10–31 March 2022, over the North-west European Continental shelf and in the adjacent North Atlantic Ocean (Fig. 1). Samples were collected from the continuous seawater supply (intake approximately at 5 m depth) and from Niskin bottles during CTD-rosette casts (20 m depth). We briefly outline the sampling of auxiliary biochemical parameters before providing a description of the dual-incubation approach developed for simultaneous assessment of phytoplankton photosynthetic rates using ^{14}C -fixation and STAF. We include a detailed description of correction approaches applied to STAF data during this study.

Biochemical parameters

Chlorophyll *a* (Chl *a*) concentration ($[\text{Chl } a]$, mg m^{-3}) at all sampling locations was analyzed fluorometrically on board the vessel. Briefly, 100 mL of seawater was filtered under low vacuum pressure onto 25 mm glass fiber (GF/F) filters, pigments were extracted in 6 mL 90% acetone at 4°C for 24 h,

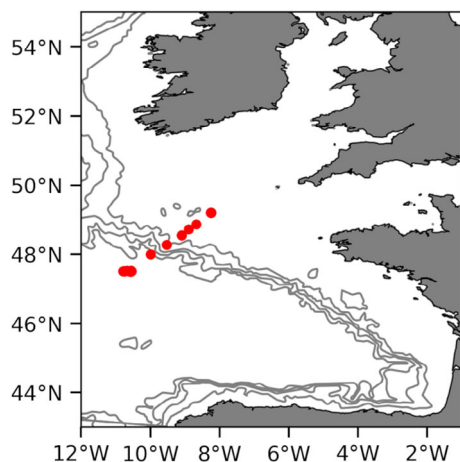


Fig. 1. Map of sampling area. All samples presented in this study were collected during research cruise DY149 on board the RRS Discovery, 10–31 March 2022. See Table 1 for more information on the individual sampling points.

and $[\text{Chl } a]$ determined on a Turner Designs Trilogy fluorometer set up with a non-acidification kit (Welschmeyer 1994).

Phytoplankton absorption spectra ($a_{\text{phy}}(\lambda)$, m^{-1}), used for the comparison of a_{phy} with STAF-derived photosynthetic excitation profiles (PEP) for spectral correction, were measured using the filter-pad approach as previously described (Bouman et al. 2020). Briefly, 0.5–1 liters of seawater were filtered onto 25 mm GFF filter which were flash-frozen in liquid nitrogen and stored at -80°C until analysis of the optical density of total particulates and detrital material remaining after extraction with 20 mL hot methanol using a dual-beam spectrophotometer (UV2101; Shimadzu Corp.) equipped with an integrating sphere. Optical densities were then converted to absorption coefficients and the absorption by phytoplankton pigments $a_{\text{phy}}(\lambda)$, m^{-1} was determined by subtracting the absorption by detrital material from the total absorption by particulates (Bouman et al. 2020).

Total dissolved inorganic carbon (DIC, $\mu\text{mol C L}^{-1}$) was determined from 250 mL samples preserved with 250 μL HgCl_2 by IR gas analysis following acidification with 10% phosphoric acid and stripping of the generated CO_2 with pure nitrogen gas using an AIRICA® DIC Analyzer (Marianda) coupled with a LICOR 840A IR $\text{CO}_2/\text{H}_2\text{O}$ Analyzer (Call et al. 2017). Accuracy and precision of DIC were verified against Certified Reference Material from Andrew Dicksons lab at SIO, yielding a typical accuracy and precision of ± 1 to $2 \mu\text{mol kg}^{-1}$ for DIC (~ 0.05 – 0.1%).

Discrete samples for dissolved nutrient concentrations were collected in acid-cleaned 50 mL Falcon tubes and stored at -20°C . Dissolved nutrients ($[\text{NO}_3^- + \text{NO}_2^-]$, $[\text{NO}_2^-]$, $[\text{PO}_4]$, $[\text{Si}]$, $\mu\text{mol L}^{-1}$) were analyzed on a SEAL QuAAtro39 autoanalyzer following standard protocols (Becker et al. 2020) and certified reference materials (Kanso, Japan). Detection limits were $0.05 \mu\text{mol L}^{-1}$ for $\text{NO}_3^- + \text{NO}_2^-$, $0.01 \mu\text{mol L}^{-1}$ for NO_2^- , $0.01 \mu\text{mol L}^{-1}$ for PO_4^{3-} , and $0.02 \mu\text{mol L}^{-1}$ for $\text{Si}(\text{OH})_4$.

Temperature and salinity of the continuous seawater supply was measured at the intake using a Seabird thermosalinograph (SBE45). For CTD-rosette profiles, temperature and salinity was recorded using a Seabird SBE 52 MP.

Single-turnover active fluorometry

All measurements were conducted using LabSTAF instruments (Fig. 2). These instruments allow for an estimation of volumetric PSII photochemical flux ($J_{\text{V,PII}}$, $\mu\text{mol e}^- \text{m}^{-3} \text{s}^{-1}$) using the absorption algorithm (Oxborough et al. 2012) with corrections for baseline fluorescence, the pigment package effect and spectral differences between measurement and actinic LEDs, as described below and in Supporting Information Material S1.

In its simplest form, the estimation of any photosynthetic rate using an optical technique depends on values of incident light (E), an estimate of how much light is absorbed (a), and an estimate of how efficiently this absorbed light energy is

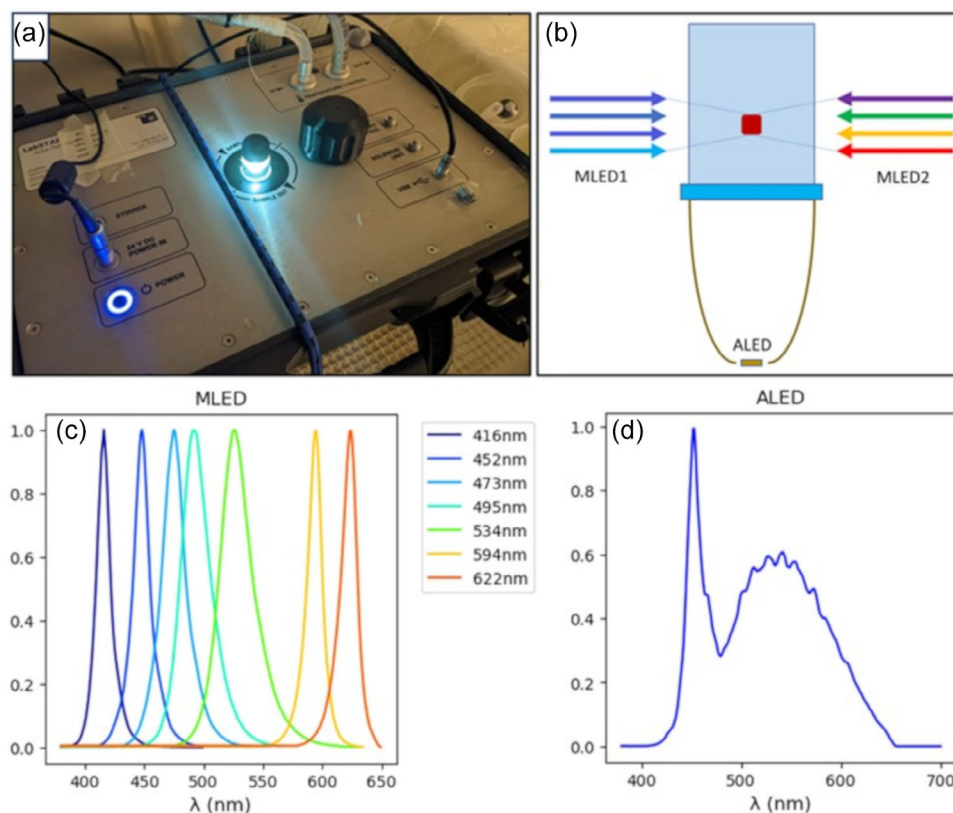


Fig. 2. The LabSTAF instrument used for dual-incubation experiments. **(A)** To facilitate dual-incubation experiments, the sampling chamber of the instrument accommodates a 25 mL scintillation vial within which a ^{14}C -spiked sample can be placed. **(B)** Single-turnover fluorescence transients are induced by measurement LEDs (MLED) from eight channels across seven wavelengths (see **C**) which provide homogeneous illumination throughout an interrogated volume of approximately 0.5 mL. Background light during the single-turnover measurement is delivered to the entire sample from a single actinic LED (ALED) via a collimating compound parabolic collector (CPC). **(C)** Normalized emission spectra of the 7 MLED wavelengths of in current LabSTAF instruments. **(D)** The spectrum of the blue-enhanced white ALED. For more details and technical specifications see Oxborough (2022).

used for photosynthesis (Φ') (Eq. 1, e.g., Sakshaug et al. 1997; Schuback et al. 2021).

$$\text{Photosynthesis} = E \times a \times \Phi', \quad (1)$$

The absorption algorithm calculates JV_{PII} from STAF data as shown in Eq. 2:

$$JV_{\text{PII}} = E \times a_{\text{LHII}} \times \Phi'_{\text{PII}}. \quad (2)$$

Within the LabSTAF instrument, the incident light (E , $\mu\text{mol photon m}^{-2} \text{s}^{-1}$) a sample is exposed to is delivered evenly to the entire sample from a blue-enhanced-white “actinic” LED (ALED, Fig. 2). Values of a_{LHII} and Φ'_{PII} are obtained from single-turnover (ST) fluorescence transients induced by a 100 μs pulse of strong excitation light from the 452 nm measuring LEDs (MLEDs) during which fluorescence emission at 680 nm is recorded at 1 MHz resolution.

The absorption coefficient a_{LHII} (m^{-1}), where LHII stands for PSII light harvesting system, quantifies light absorption by

pigments connected to functional PSII reaction centers (Oxborough et al. 2012). It is calculated following Eq. 3:

$$a_{\text{LHII}} = K_a \times \frac{F_m \times F_o}{F_v}. \quad (3)$$

Here, K_a is an instrument type specific constant with units of m^{-1} , derived from oxygen flash yield (Oxborough et al. 2012) or simultaneous STAF and O_2 -evolution measurements (Boatman et al. 2019). F_o and F_m are the minimum and maximum fluorescence in the dark-regulated state while F_v is the variable fluorescence derived as $F_m - F_o$.

The PSII photochemical efficiency parameter (Φ'_{PII}) in Eq. 2 defines the proportion of photons absorbed by pigments connected to functional PSII reaction centers that result in photochemistry. It is estimated as F_q'/F_m' (Genty et al. 1989) where F_q'/F_m' is the variable fluorescence ($F_q' = F_m' - F'$) normalized to the maximum fluorescence (F_m') in the light-regulated state, and F' is the minimum fluorescence in the light regulated state.

More detailed descriptions of the absorption algorithm are provided by Oxborough (2022), Tortell et al. (2023), and in Supporting Information Material S1.

The most accurate derivation of JV_{PH} relies on the application of several important correction approaches, described below. Note that the incorporation of these corrections into the above equations, including necessary unit conversion, are further described in Supporting Information material S1.

Spectral correction

All STAF-based estimates of absorption-cross sections or absorption coefficients are spectrally dependent (e.g., Schuback et al. 2021, ch. 3.5 in Tortell et al. 2023). This means they are specific to the wavelengths of the MLED used for the ST pulse from which they are derived (most commonly 452 nm).

Consequently, if these parameters are to be used for calculations of JV_{PH} specific to the intensity of the spectrally different ALED providing illumination in the sample chamber, or if rates of JV_{PH} realized at in situ light availability are to be derived, spectral correction is required (Sakshaug et al. 1997; Moore et al. 2006). Spectral correction requires knowledge of the emission spectra of both light sources relative to the spectral distribution of light absorption by phytoplankton. In the past, this necessitated additional measurements of phytoplankton absorption spectra (a_{phy}) or, ideally, Chl *a* fluorescence excitation spectra (Moore et al. 2006; Silsbe et al. 2015; Hughes et al. 2020). In LabSTAF instruments an automated spectral correction approach utilizing routine measurements of photochemical excitation profiles (PEP) has been implemented. Here, ST fluorescence transients are induced with MLEDs at seven different wavelengths (416, 452, 473, 495, 534, 595, 622 nm; Fig. 3) and the resulting wavelength-specific values of variable fluorescence (F_v) are used to construct the PEP. Together with information on spectral emission of MLED and ALED, these data are used to derive a correction factor (cPEP; Eq. 4; Fig. 3).

$$cPEP = \frac{\int_{400}^{700} PEP(\lambda) ALED(\lambda) d\lambda \times \int_{400}^{700} MLED_{452nm}(\lambda) d\lambda}{\int_{400}^{700} PEP(\lambda) MLED_{452nm}(\lambda) d\lambda \times \int_{400}^{700} ALED(\lambda) d\lambda} \quad (4)$$

In our dataset, values of cPEP ($n = 44$) ranged from 0.45 to 0.61 (mean = 0.51). The magnitude of this correction is in line with what has been observed in previous studies (Silsbe et al. 2015) and its limited range can be explained by the limited variability in physical and biochemical conditions leading to a limited heterogeneity of phytoplankton community composition encountered during this study.

Importantly, the approach facilitates automated spectral correction without the need for auxiliary measurements of a_{phy} (Fig. 3).

Spectra of the MLEDs and ALED were acquired inside the LabSTAF sample chamber using an intensity-calibrated OtO Smart Engine spectrometer and an OceanOptics

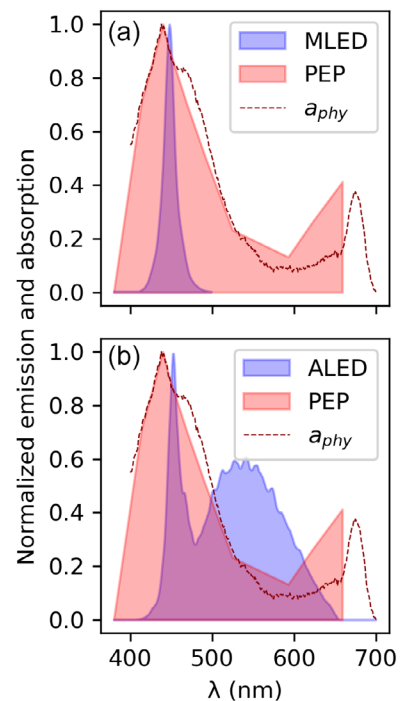


Fig. 3. LED emission and phytoplankton absorption spectra used for spectral correction. **(A)** The emission spectrum of the 452 nm MLED used for routine measurement ST pulse (MLED_{452nm}) and **(B)** the emission spectrum of the blue-enhanced white ALED. Both LED spectra are shown relative to the PEP constructed from F_v values measured at seven wavelengths and, for comparison, the phytoplankton absorption spectrum (a_{phy}) from samples (a_{phy}) taken at UW36 and analyzed using the filter-pad method. The correction factor calculated for this sample is 0.46 using the PEP data and 0.45 if a_{phy} measured using the filter-pad method is used. For ease of comparison, all spectra are normalized to their maximum values. Note that the larger discrepancy of PEP and a_{phy} above 600 nm does not affect the derivation of the spectral correction factor because the background actinic light (or a typical light spectrum in situ) provides little irradiance in this spectral region.

USB2000+ spectrometer that was cross-calibrated for intensity using an OceanOptics LS-1 tungsten-halogen lamp. The photosynthetically-active radiation (PAR) provided by each light source was measured using a Walz US-SQS/L spherical micro quantum sensor and calibrated Fluka multimeter, and corrected using the quantum sensor's specific spectral response.

Baseline fluorescence correction

Baseline fluorescence is non-inducible fluorescence emanating primarily from Chl *a* molecules not functionally associated with reaction centers of photosynthetically active PSII (Boatman et al. 2019; Schuback et al. 2021). It leads to an equal increase in values of F_o and F_m and thus results in decreased values of F_v/F_m which are typically associated with nutrient limitation (Greene et al. 1994; Behrenfeld and Milligan 2013). The presence of baseline fluorescence perturbs the interpretation of F_v/F_m as the maximum and F_q'/F_m' as the

realized photochemical efficiency of PSII if applied in the calculation of JV_{PII} using the absorption algorithm or other approaches (Boatman et al. 2019; Schuback et al. 2021).

We here followed the approach suggested by Boatman et al. (2019) and calculated baseline fluorescence (F_b) in the dark-regulated-state as

$$F_b = F_m - \frac{F_v}{F_v/F_{mc}}, \quad (5)$$

where F_v/F_{mc} is the assumed “intrinsic” value for photochemically active PSII complexes within the sample and was here assumed to be 0.5 (see Supporting Information Material S2 for a sensitivity analysis on this assumption). In the light-regulated state, and with the prime (') suffix denoting light-regulated conditions, we calculated estimates of F_b' as.

$$F_b' = F_b \times F_m'/F_m, \quad (6)$$

which assumes that light exposure leads to the same of quenching in F_b as in F_m .

Using the absorption algorithm (Eqs. 2, 3), both a_{LHII} and F_q'/F_m' are affected by baseline fluorescence. Within the present dataset correction for the estimated baseline fluorescence reduced values of a_{LHII} by 4–69% (mean = 32%, $n = 44$) and increased values of F_q'/F_m' by 1–54% (mean = 16%, $n = 44$), resulting in decreases in JV_{PII} from 3% to 52% (mean = 23%, $n = 44$). As in Boatman et al. (2019) we did not observe a significant difference in baseline corrected values of JV_{PII} when using quenched (Eq. 6) or unquenched (Eq. 5) values of F_b in our corrections, however we caution that quenching of F_b could be more significant under other conditions, for example, iron limitation. A further critical analysis of the effect of baseline fluorescence correction on values of JV_{PII} and $\Phi_{e,C}$ and the choice of 0.5 as F_v/F_{mc} is included in Supporting Information Material S2 and the discussion.

Package effect correction

A prerequisite of the absorption algorithm is that the ratio between light energy used for photochemistry in PSII and light energy emitted as fluorescence from PSII stay within a narrow range (Oxborough et al. 2012). This can be significantly distorted by the pigment package effect (Fig. 4), necessitating corrections (Boatman et al. 2019). The pigment package effect is a result of the self-shading of Chl *a* molecules tightly packed inside phytoplankton cells and is thus more pronounced in large or highly pigmented cells (Fig. 4B). In addition to reducing light absorption per Chl *a* molecule (Ciotti et al. 2002), packaging directly affects the re-emission of fluorescence, because the red absorption peak of Chl *a* partly overlaps with the emission peak of fluorescence (Fig. 4A). Consequently, the reabsorption of fluorescence decreases the fluorescence signal. Boatman et al. (2019)

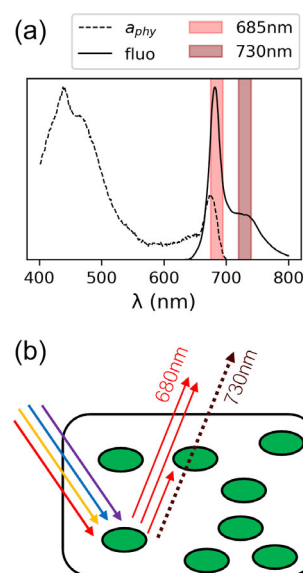


Fig. 4. The dual-waveband measurement (DWM) approach used to correct for the effects of pigment packaging. **(A)** Spectra of Chl *a* fluorescence emission (solid line, data taken from Pedrós et al. 2008) and phytoplankton absorption (a_{phy} , dashed line, sample taken at UW36 and analyzed using the filter-pad method). Fluorescence emission is measured after transmission through a 685 ± 10 nm full width-half max (FWHM) bandpass filter, indicated by the red shaded area. In this spectral region the fluorescence emission is strong and specific to PSII, however, some fluorescence will be reabsorbed. The dual-waveband approach utilizes an additional measurement of fluorescence after transmission through a 730 ± 10 nm FWHM bandpass filter, indicated by the dark-red shaded area. In this spectral region the fluorescence emission is weaker, however, no reabsorption by photosynthetic pigments occurs. The ratio 730 nm/685 nm should thus provide a proxy for reabsorption of Chl *a* fluorescence. All spectra are normalized to their respective maximum values. For more details and technical specifications see Oxborough (2022). **(B)** Schematic diagram of the pigment package effect in a phytoplankton cell. Light energy within the PAR spectrum is absorbed by pigments and some energy absorbed by Chl *a* molecules of PSII is re-emitted as fluorescence with an emission peak at 680–685 nm. A variable proportion of this fluorescence is re-absorbed by *cha*, with the extent of reabsorption depending on optical characteristics of the cell (e.g., cell size and pigment density). Reabsorption at 730 nm is extremely low.

introduced an approach to obtain a proxy for pigment packaging based on detection of fluorescence emission at two wavebands. The so-called dual-waveband measurement (DWM) uses the ratio of fluorescence detected at 730 nm (where reabsorption is low) to 685 nm (where reabsorption is higher) as a proxy for pigment packaging (Fig. 4). The correction factor (cPEC) is then derived as DWM relative to a calibration standard and applied to values of a_{LHII} to correct for varying levels of pigment packaging. Values of cPEC in our dataset ($n = 44$) range from 0.48 to 0.77 (mean = 0.53).

Dual-incubation experiments

The dual-incubation experiments tested in the present study are facilitated by the relatively large sample chamber

incorporated within LabSTAF (25 mm diameter and 56 mm height). A ^{14}C -spiked sample, contained within a scintillation vial (23 mm diameter, 24 mL volume) can be incubated within the LabSTAF sample chamber and STAF measurements can be made throughout the incubation period (Fig. 2A). ^{14}C -uptake and $J_{\text{V}_{\text{P}}}$ are therefore measured simultaneously on the same sample, avoiding methodological bias such as different incubation times and light sources, which are common in experiments where the two rates are measured in parallel (e.g., Lawrenz et al. 2013; Hughes et al. 2018b).

Samples were inserted into the LabSTAF sampling chamber inside a 24 mL scintillation vial surrounded by MQ water and held in place by a custom-made sample chamber cap. A blank of 0.2 μm filtrate was first run on each instrument. After collection, samples were kept at in situ temperature and low light for ca 20 min until the start of incubations. Un-spiked samples were then exposed to a STAF measurement protocol to determine a photosynthetic excitation profile (PEP), dual wavelengths correction factor (cPEC), and ST parameter in the dark-regulated state (i.e., F_o , F_m). After this “dark acquisition”, the samples were spiked with 20–30 μCi ^{14}C sodium bicarbonate solution and incubated with background irradiances switched on to determine ST parameters in the light-regulated state (i.e., F' , F'_m). An additional vial was spiked and incubated in the dark. After incubation, ^{14}C -fixation was determined by filtering a (sub-)sample (7–10 mL) onto 25 mm GF/F filter and placing the filter into a scintillation vial containing 500 μL 2 mol L^{-1} HCl over night to remove all inorganic carbon. Total ^{14}C spike in each incubation vial was determined from triplicate 100 μL aliquots pipetted into scintillation vials containing 500 μL 0.1 mol L^{-1} NaOH. Five-milliliter scintillation cocktail (Ultima Gold) was added to each scintillation vial and counts obtained by the shipboard liquid scintillation counter as disintegrations per minute (DPM) using automatic quench correction and a counting time of 5 min. Rates of ^{14}C -fixation into particulate organic carbon (PO^{14}C , $\mu\text{mol C L}^{-1} \text{h}^{-1}$) were calculated as

$$\text{PO}^{14}\text{C} = \frac{\text{DIC} \times (\text{DPM}_{\text{sample}} - \text{DPM}_{\text{dark}}) \times 1.05}{\text{DPM}_{\text{TC}} \times t}, \quad (7)$$

where DIC is the concentrations of dissolved inorganic carbon ($\mu\text{mol C L}^{-1}$). $\text{DPM}_{\text{sample}}$, DPM_{dark} , and DPM_{TC} are DPM of sample, dark incubation, and total counts. t is incubation time in hours and the value of 1.05 corrects for the fractionation against ^{14}C relative to ^{12}C . In our set of experiments, DPM_{dark} was with 47 DPM mL^{-1} (std = 16 DPM mL^{-1} , $n = 55$) 15% of the average $\text{DPM}_{\text{sample}}$ values. The general approach described above was used to generate three datasets:

Dataset 1. Time-course experiments. The experimental design of dataset 1 was aimed at testing the effect of incubation time on the coupling of ^{14}C -fixation and $J_{\text{V}_{\text{P}}}$ as ^{14}C -fixation decreases from gross to net with increasing time (Halsey et al. 2011). At 4 stations samples were taken from

CTD casts at 20 m depth (Tables 1, 2). Samples were split and incubated in two instruments, at light-limiting (50 $\mu\text{mol photon m}^{-2} \text{s}^{-1}$) and light saturating (300 $\mu\text{mol photon m}^{-2} \text{s}^{-1}$) conditions. Subsamples of 8 mL were filtered from each incubation after 0.5, 1, and 2 h incubation times.

Dataset 2. Light-level experiments. The experimental design of dataset 2 was aimed at obtaining a large dataset of $\Phi_{\text{e,C}}$ values at light-limited and light-saturated conditions. At 10 stations, samples were taken from CTD casts at 20 m depth and incubated for 2 h at light-limited (50 $\mu\text{mol photon m}^{-2} \text{s}^{-1}$) and light saturated (300 $\mu\text{mol photon m}^{-2} \text{s}^{-1}$) conditions. At seven stations, samples were taken from the continuous seawater supply (ca 5 m depth) at 06:00 h local time and incubated for 2 h at light-limited (30 $\mu\text{mol photon m}^{-2} \text{s}^{-1}$) and light-saturated (300 $\mu\text{mol photon m}^{-2} \text{s}^{-1}$) conditions (Tables 1, 3).

Dataset 3. diurnal cycle experiment. At one station, dual-incubation experiments were performed on samples taken from the continuous seawater supply at 3 h intervals over a diurnal cycle. Here, the incubation light level in one instrument was kept constant at 50 $\mu\text{mol photon m}^{-2} \text{s}^{-1}$, while the light level in the second instrument was set to the estimated light intensity experienced by phytoplankton at the time and depth of sampling (Tables 1, 4). Incubations lasted for 2 h.

Results

In the following, we briefly describe the environmental conditions encountered during our sampling before presenting the magnitude, range and trends observed in $\Phi_{\text{e,C}}$ values from dual-incubation experiments.

Environmental assessment of sampling area

The area visited during research cruise DY149 was confined to a relatively small part of the North Atlantic Ocean and adjacent continental shelf to the west of northern Europe. Sampling locations included on- and off-shelf stations and thus had some variability in nutrient concentrations and phytoplankton biomass (Fig. 1; Table 1). Broadly, macronutrients were replete across all sampling points and chlorophyll concentrations reflected the early stage of the annual spring bloom as the system was in the early stages of stratification in spring.

Across our 23 sampling points, [Chl *a*] ranged from 0.61 to 2.95 mg m^{-3} (mean = 1.08 mg m^{-3}), temperature ranged from 11°C to 12.5°C (mean = 11.8°C), salinity ranged from 35.33 to 35.57 PSU (mean = 35.48 PSU), DIC ranged from 2128 to 2150 $\mu\text{mol L}^{-1}$ (mean = 2139 $\mu\text{mol L}^{-1}$), $[\text{NO}_3 + \text{NO}_2]$ ranged from 2.72 to 6.97 $\mu\text{mol L}^{-1}$ (mean = 5.87 $\mu\text{mol L}^{-1}$), $[\text{NO}_2]$ ranged from 0.04 to 0.15 $\mu\text{mol L}^{-1}$ (mean = 0.1 $\mu\text{mol L}^{-1}$), [Si] ranged from 1.43 to 2.5 $\mu\text{mol L}^{-1}$ (mean = 2.19 $\mu\text{mol L}^{-1}$), $[\text{PO}_4]$ ranged from 0.23 to 0.43 $\mu\text{mol L}^{-1}$ (mean = 0.38 $\mu\text{mol L}^{-1}$) (Table 1).

Table 1. Environmental characterization of sampling points. Samples for dual-incubation experiments ($n = 60$) were collected at 23 stations. Dataset 1 = time-course experiment; dataset 2 = light-level experiment; dataset 3 = diurnal experiment. See method section for more details on experiments and parameters and Supporting Information material S2 for a correlation matrix between environmental parameters and measured photophysiological parameters and rates.

DS	UTC		m	Sample	°N	°W	mg m ⁻³	°C	PSU	μmol L ⁻¹	μmol L ⁻¹				F _v /F _m
	Date	Time									Depth	Lat	Long	Chl <i>a</i>	
1	18 Mar	18:10	23	CTD6	47.52	10.68	0.83	12.0	35.56	2139	6.83	2.31	0.04	0.40	0.43
1	19 Mar	10:10	22	CTD7	47.52	10.56	0.75	12.1	35.57	2137	6.35	2.07	0.14	0.38	0.45
1	20 Mar	10:55	21	CTD9	47.50	10.55	0.80	12.1	35.57	2148	6.05	2.08	0.13	0.38	0.41
1	20 Mar	16:40	23	CTD10	47.50	10.61	1.01	12.1	35.57	2134	5.56	1.89	0.13	0.36	0.44
2	22 Mar	09:50	22	CTD13	47.50	10.55	0.90	12.0	35.56	2138	6.16	2.18	0.04	0.40	0.45
2	23 Mar	09:40	22	CTD14	49.20	8.25	0.73	11.0	35.36	2144	5.70	2.37	0.15	0.42	0.47
2	24 Mar	09:10	22	CTD16	49.20	8.25	0.92	11.0	35.36	2145	6.26	2.46	0.14	0.42	0.47
2	25 Mar	12:40	23	CTD20	48.72	8.89	2.95	11.7	35.47	2128	4.84	1.74	0.05	0.35	0.49
2	26 Mar	09:10	22	CTD21	48.54	9.09	1.75	12.0	35.55	2130	5.71	2.22	0.10	0.37	0.48
2	27 Mar	07:30	22	CTD23	48.27	9.53	1.47	11.9	35.54	2138	6.42	2.15	-	0.41	0.49
2	22 Mar	06:00	7	UW28	47.50	10.55	0.86	11.2	35.33	2150	6.42	2.50	0.15	0.42	0.43
2	23 Mar	06:00	7	UW32	49.20	8.24	0.61	11.8	35.45	2145	4.62	1.85	0.05	0.33	0.44
2	24 Mar	06:00	7	UW36	49.21	8.25	0.71	12.1	35.53	2148	6.97	2.47	0.10	0.40	0.43
2	25 Mar	06:00	7	UW40	48.87	8.68	1.22	12.0	35.52	2130	6.78	2.29	0.14	0.41	0.46
2	26 Mar	06:00	7	UW44	48.55	9.10	1.22	12.5	35.55	2139	6.73	2.43	0.10	0.38	0.45
2	27 Mar	06:00	7	UW48	48.27	9.53	1.57	12.5	35.55	2140	4.90	2.12	0.06	0.30	0.46
2	28 Mar	06:00	7	UWS2	48.00	10.00	0.78	11.9	35.41	2140	2.72	1.43	0.05	0.23	0.40
3	21 Mar	06:00	7	TP1	47.52	10.55	0.83	12.5	35.55	-	-	-	-	-	0.43
3	21 Mar	09:00	7	TP2	47.49	10.57	-	12.4	35.52	-	-	-	-	-	0.43
3	21 Mar	12:00	7	TP3	47.50	10.59	0.91	12.4	35.55	2135	6.29	2.50	0.10	0.43	0.33
3	21 Mar	15:00	7	TP4	47.50	10.74	-	12.5	35.52	-	-	-	-	-	0.34
3	21 Mar	18:00	7	TP5	47.50	10.74	0.83	12.6	35.33	2135	6.25	2.48	0.10	0.42	0.38
3	21 Mar	21:00	7	TP6	47.51	10.79	-	12.7	35.54	-	-	-	-	-	0.40

Within the dataset, no strong correlations between [Chl *a*] and any of the physical and chemical variables listed were observed (Supporting Information Material S3).

Magnitude and variability of $\Phi_{e,C}$

Overall, observed values of $\Phi_{e,C}$ ranged from 3.0 to 12.1 e⁻ C⁻¹ with a mean 7.0 e⁻ C⁻¹ ($n = 60$, Tables 2–4). Observed variability followed some expected trends, as explained for each dataset below. Values of $\Phi_{e,C} < 4$ e⁻ C⁻¹ cannot be explained physiologically, given that during the photosynthetic process four charge separations in PSII are necessary for the splitting of two water molecules leading to the evolution of one O₂ and a maximum of one CO₂ is fixed per O₂ evolved (e.g., Williams and Robertson 1991). Values of $\Phi_{e,C}$ below 4 are thus likely to result from remaining errors in the calculation of either carbon fixation or J_{V_{PII}}, specifically overestimation of gross carbon fixation or underestimation of J_{V_{PII}}. Considering that our 2 h ¹⁴C-fixation experiments likely underestimated gross carbon fixation (i.e., some initially fixed ¹⁴C is likely lost by excretion or respiration), values of $\Phi_{e,C} < 4$ e⁻ C⁻¹ are more likely due to underestimation of J_{V_{PII}}. In the

discussion, we critically assess the three correction approaches applied in the derivation of J_{V_{PII}} values in this study, and whether either of them could have led to an under-estimation of J_{V_{PII}}. It is further worth noting that the two instances of $\Phi_{e,C} < 4$ e⁻ C⁻¹ occurred at stations with low biomass (CTD7 and CTD9, Table 1), which could have affected the accuracy of our ¹⁴C-fixation experiments.

Time-course experiments

In all dual-incubation time-course experiments $\Phi_{e,C}$ increased with increasing incubation time (Fig. 5E,F; Table 2). The increase in $\Phi_{e,C}$ is caused by a reduction in the measured rate of ¹⁴C-fixation (Fig. 5C,D; Table 2), most probably because initially fixed ¹⁴C is increasingly respired or lost as DOC during the longer incubation times (e.g., Halsey et al. 2011). Variability in J_{V_{PII}} over the incubation period was small, with a trend of increasing rate with increasing incubation time observed at light saturation (Fig. 5A,B; Table 2).

The average increase in $\Phi_{e,C}$ was 84% when comparing 0.5 h with 2 h incubation times. However, the average increase in $\Phi_{e,C}$ from 0.5 to 1 h incubation (56%) was much

Table 2. Photophysiological parameters, photosynthetic rates, and $\Phi_{e,c}$ measured during the time-course experiments of dataset 1. Samples were collected from 20 m depth at four stations—see Table 1 for environmental parameter. At each station, dual-incubation experiments were performed for three durations (Incub time, h) and two light levels (LL, $\mu\text{mol photon m}^{-2} \text{s}^{-1}$). Values of σ_{Pll} and $\sigma_{\text{Pll}'}$ (nm PSII^{-1}) are not spectrally corrected and therefore specific to 452 nm. The value of F_v/F_m (unitless) is not corrected for baseline fluorescence and should thus be sensitive to the effects of nutrient stress. The value of $F_q'/F_{m,c}'$ (unitless) is corrected for baseline fluorescence, indicated by the subscript c. It is therefore an estimate of the realized quantum yield of charge separation in PSII, specific to light absorbed by pigment functionally associated to PSII. The absorption coefficient for pigments functionally associated to PSII, a_{LHII} (m^{-1}), is calculated following Eq. 3 and corrected for the effects of baseline fluorescence, pigment packaging, and spectral differences between MLED and ALED (see also Supporting Information Material S1). JV_{Pll} ($\mu\text{mol e}^{-} \text{m}^{-3} \text{s}^{-1}$) is calculated following Eq. 2 and POC production ($\mu\text{mol C m}^{-3} \text{s}^{-1}$) measured using ^{14}C , as described in the methods. The electron requirement for carbon fixation ($\Phi_{e,c}$, $\text{e}^{-} \text{C}^{-1}$) is derived as $JV_{\text{Pll}}/\text{POC}$.

Sample	h	$\mu\text{mol photon m}^{-2} \text{s}^{-1}$	nm PSII^{-1}		F_v/F_m	$F_q'/F_{m,c}'$	m^{-1}	$\mu\text{mol e}^{-} \text{m}^{-3} \text{s}^{-1}$	$\mu\text{mol C m}^{-3} \text{s}^{-1}$	$\text{e}^{-} \text{C}^{-1}$
	Incub time	LL	σ_{Pll}	$\sigma_{\text{Pll}'}$						
CTD6	0.5	50	6.9	5.6	0.43	0.38	0.007	0.132	0.023	5.8
CTD6	1	50	6.9	5.6	0.43	0.38	0.007	0.136	0.023	6.0
CTD6	2	50	6.9	5.6	0.43	0.38	0.007	0.137	0.021	6.4
CTD6	0.5	300	7.0	2.8	0.43	0.12	0.007	0.232	0.041	5.7
CTD6	1	300	7.0	2.8	0.43	0.12	0.007	0.240	0.039	6.2
CTD6	2	300	7.0	2.8	0.43	0.12	0.007	0.247	0.031	7.9
CTD7	0.5	50	7.0	5.4	0.45	0.39	0.006	0.124	0.028	4.4
CTD7	1	50	7.0	5.4	0.45	0.39	0.006	0.121	0.023	5.3
CTD7	2	50	7.0	5.4	0.45	0.39	0.006	0.123	0.021	5.9
CTD7	0.5	300	6.9	3.3	0.45	0.16	0.006	0.270	0.071	3.8
CTD7	1	300	6.9	3.3	0.45	0.16	0.006	0.284	0.040	7.1
CTD7	2	300	6.9	3.3	0.45	0.16	0.006	0.294	0.038	7.8
CTD9	0.5	50	7.7	6.0	0.41	0.46	0.006	0.128	0.043	3.0
CTD9	1	50	7.7	6.0	0.41	0.46	0.006	0.132	0.018	7.3
CTD9	2	50	7.7	6.0	0.41	0.46	0.006	0.135	0.017	8.2
CTD9	0.5	300	7.6	3.4	0.41	0.17	0.006	0.278	0.068	4.1
CTD9	1	300	7.6	3.4	0.41	0.17	0.006	0.288	0.041	7.0
CTD9	2	300	7.6	3.4	0.41	0.17	0.006	0.297	0.037	8.1
CTD10	0.5	50	7.6	6.2	0.44	0.41	0.009	0.188	0.044	4.2
CTD10	1	50	7.6	6.2	0.44	0.41	0.009	0.185	0.026	7.1
CTD10	2	50	7.6	6.2	0.44	0.41	0.009	0.186	0.018	10.6
CTD10	0.5	300	7.5	2.8	0.44	0.11	0.009	0.271	0.065	4.2
CTD10	1	300	7.5	2.8	0.44	0.11	0.009	0.277	0.045	6.1
CTD10	2	300	7.5	2.8	0.44	0.11	0.009	0.284	0.042	6.8

higher than the average increase observed when comparing 1–2 h incubation (18%).

Light-level experiments

At 17 stations, 2 h dual-incubations were performed under light limiting (30 and 50 $\mu\text{mol photon m}^{-2} \text{s}^{-1}$ for UW and CTD samples, respectively) and light saturating (200 and 300 $\mu\text{mol photon m}^{-2} \text{s}^{-1}$ for UW and CTD samples, respectively) irradiances. Light-response curves, run on a separate LabSTAF instrument, confirmed that the highlight value was indeed above the E_k of each sample. Values of $\Phi_{e,c}$ measured under light-limitation range from 5.0 to 10.6 $\text{e}^{-} \text{C}^{-1}$ (mean = 7.3 $\text{e}^{-} \text{C}^{-1}$, $n = 17$; Table 3) while values at light-saturation range from 6.1 to 11.4 $\text{e}^{-} \text{C}^{-1}$ (mean = 8.1 $\text{e}^{-} \text{C}^{-1}$,

$n = 17$; Table 3). As shown in Fig. 6, for paired measurements, $\Phi_{e,c}$ measured under light-saturation was higher than $\Phi_{e,c}$ measured under light-limitation ($t(16) = 1.74$; $p = 0.028$), as has been previously observed in other studies (Corno et al. 2006; Fujiki et al. 2007; Schuback et al. 2015, 2017; Zhu et al. 2017).

Diurnal experiment

On 21 March 2022, dual-incubation experiments were performed at 3 h intervals using samples collected from the continuous seawater supply. During the sampling period, the ship remained within a small geographic area off the shelf (Table 1), where temperature (12.4–12.7°C) and salinity

Table 3. Photophysiological parameters, photosynthetic rates, and $\Phi_{e,c}$ measured during the light level experiments of dataset 2. Samples were collected from the CTD-rosette at 20 m depth at six stations and the continuous underway water supply (UW, intake ca 5 m depth) at seven stations—see Table 1 for environmental parameter. At each station, dual-incubation experiments were performed at two light levels (LL, $\mu\text{mol photon m}^{-2} \text{s}^{-1}$) for 2 h. Values of σ_{PII} and $\sigma_{\text{PII}'}$ (nm PSII^{-1}) are not spectrally corrected and therefore specific to 452 nm. The value of F_v/F_m (unitless) is not corrected for baseline fluorescence and should thus be sensitive to the effects of nutrient stress. The value of F_q'/F_{mc}' (unitless) is corrected for baseline fluorescence, indicated by the subscript c. It is therefore an estimate of the realized quantum yield of charge separation in PSII, specific to light absorbed by pigments functionally associated to PSII. The absorption coefficient for pigments functionally associated to PSII, a_{LHII} (m^{-1}), is calculated following Eq. 3 and corrected for the effects of baseline fluorescence, pigment packaging, and spectral differences between MLED and ALED (see also Supporting Information Material S1). JV_{PII} ($\mu\text{mol e}^{-} \text{m}^{-3} \text{s}^{-1}$) is calculated following Eq. 2, the error shown is the standard deviation of JV_{PII} measured throughout the 2 h incubation time. Particulate organic carbon (POC) production ($\mu\text{mol C m}^{-3} \text{s}^{-1}$) was measured using ^{14}C , as described in the methods, and the error shown is derived from duplicate ^{14}C -fixation filtrations for each sample. The electron requirement for carbon fixation ($\Phi_{e,c}$, $\text{e}^{-} \text{C}^{-1}$) is derived as $JV_{\text{PII}}/\text{POC}$ and the error is the propagated error from JV_{PII} and POC.

Sample	$\mu\text{mol photon m}^{-2} \text{s}^{-1}$		nm PSII^{-1}		F_v/F_m	F_q'/F_{mc}'	m^{-1}	$\mu\text{mol e}^{-} \text{m}^{-3} \text{s}^{-1}$	$\mu\text{mol C m}^{-3} \text{s}^{-1}$	$\text{e}^{-} \text{C}^{-1}$
	LL		σ_{PII}	$\sigma_{\text{PII}'}$						
CTD13	50		7.6	6.5	0.45	0.38	0.007	0.13 ± 0.01	0.02 ± 0.001	6.0 ± 0.4
CTD13	300		7.7	3.1	0.46	0.12	0.008	0.27 ± 0.03	0.04 ± 0.004	6.3 ± 0.9
CTD14	50		6.6	5.6	0.46	0.37	0.006	0.11 ± 0.01	0.02 ± 0.001	5.0 ± 0.5
CTD14	300		6.8	3.2	0.47	0.16	0.005	0.26 ± 0.05	0.03 ± 0.000	7.7 ± 1.6
CTD16	50		7.0	6.4	0.47	0.39	0.008	0.15 ± 0.01	0.02 ± 0.000	7.9 ± 0.5
CTD16	300		6.8	3.2	0.48	0.13	0.008	0.32 ± 0.04	0.05 ± 0.003	6.3 ± 1.0
CTD20	50		5.0	4.6	0.48	0.45	0.027	0.60 ± 0.03	0.07 ± 0.000	8.8 ± 0.5
CTD20	300		4.8	3.4	0.49	0.25	0.023	1.79 ± 0.16	0.17 ± 0.003	10.6 ± 1.0
CTD21	50		6.4	5.9	0.49	0.40	0.013	0.26 ± 0.01	0.03 ± 0.001	7.9 ± 0.4
CTD21	300		6.7	3.9	0.48	0.21	0.012	0.74 ± 0.07	0.09 ± 0.002	8.5 ± 1.1
CTD23	50		5.6	4.5	0.48	0.38	0.009	0.16 ± 0.02	0.02 ± 0.000	7.4 ± 0.7
CTD23	300		5.4	3.0	0.49	0.21	0.012	0.72 ± 0.07	0.08 ± 0.002	9.1 ± 1.0
UW28	30		7.0	6.4	0.43	0.43	0.007	0.09 ± 0.00	0.01 ± 0.001	8.5 ± 1.1
UW28	200		6.9	4.3	0.43	0.21	0.007	0.30 ± 0.03	0.03 ± 0.002	8.8 ± 1.0
UW32	30		6.4	5.9	0.45	0.39	0.005	0.06 ± 0.00	0.01 ± 0.000	7.9 ± 0.7
UW32	200		6.5	3.6	0.44	0.17	0.004	0.15 ± 0.02	0.02 ± 0.000	8.2 ± 0.9
UW36	30		6.0	5.5	0.43	0.37	0.005	0.05 ± 0.00	0.01 ± 0.002	5.0 ± 1.0
UW36	200		5.9	3.9	0.43	0.22	0.004	0.18 ± 0.02	0.03 ± 0.001	6.1 ± 0.8
UW40	30		5.4	4.7	0.46	0.44	0.008	0.11 ± 0.01	0.01 ± 0.001	9.3 ± 0.9
UW40	200		5.3	4.4	0.46	0.34	0.010	0.69 ± 0.05	0.06 ± 0.000	11.4 ± 0.9
UW44	30		6.3	5.1	0.45	0.38	0.012	0.14 ± 0.01	0.02 ± 0.002	6.9 ± 0.6
UW44	200		6.3	3.7	0.45	0.23	0.012	0.55 ± 0.06	0.07 ± 0.002	7.3 ± 0.8
UW48	30		5.8	4.8	0.46	0.42	0.011	0.14 ± 0.01	0.02 ± 0.003	7.4 ± 1.4
UW48	200		5.8	3.3	0.46	0.23	0.011	0.51 ± 0.08	0.06 ± 0.002	8.7 ± 1.4
UW52	30		6.8	6.1	0.40	0.42	0.005	0.06 ± 0.00	0.01 ± 0.000	5.0 ± 0.4
UW52	200		6.7	4.7	0.40	0.26	0.005	0.29 ± 0.03	0.03 ± 0.000	8.4 ± 0.8

(35.3–35.6 PSU) continuously recorded at the water intake stayed within a narrow range.

The left column of Fig. 7 shows data for dual-incubations performed at $30 \mu\text{mol photon m}^{-2} \text{s}^{-1}$ at each of the sampling points. JV_{PII} at $30 \mu\text{mol photon m}^{-2} \text{s}^{-1}$ stayed within a relatively narrow range ($0.07\text{--}0.11 \mu\text{mol e}^{-} \text{m}^{-3} \text{s}^{-1}$), with an increase in the late afternoon, indicating acclimation of the photosynthetic process to available light (Fig. 7A, Table 4). In contrast, rates of ^{14}C -fixation, measured at a constant light intensity of $30 \mu\text{mol photon m}^{-2} \text{s}^{-1}$, decreased by 53%

throughout the day, with a slight increase at the last sampling point after dusk (Fig. 7B; Table 4). This decrease can be explained by circadian shifts in cellular metabolism leading to the allocation of photosynthetic energy away from ^{14}C -fixation and growth (Bruyant et al. 2005; Schuback and Tortell 2019). The resulting values of $\Phi_{e,c}$ thus remain low in the first half of the day and more than double in the late afternoon (Fig. 7C; Table 4).

The right column of Fig. 7 shows data from dual-incubation experiments performed at the estimated approximate light

Table 4. Photophysiological parameters, photosynthetic rates, and $\Phi_{e,c}$ measured during the diurnal experiment of dataset 3. Samples were collected from the continuous underway water supply (UW, intake ca 5 m depth) in 3 h intervals—see Table 1 for environmental parameter. At each timepoint (TP), dual-incubation experiments were performed at 2 light levels (LL, $\mu\text{mol photon m}^{-2} \text{s}^{-1}$) for 2 h. Values of σ_{PII} and $\sigma_{\text{PII}'}$ (nm PSII^{-1}) are not spectrally corrected and therefore specific to 452 nm. The value of F_v/F_m (unitless) is not corrected for baseline fluorescence and should thus be sensitive to the effects of nutrient stress. The value of F_q'/F_{mc}' (unitless) is corrected for baseline fluorescence, indicated by the subscript c. It is therefore an estimate of the realized quantum yield of charge separation in PSII, specific to light absorbed by pigments functionally associated to PSII. The absorption coefficient for pigments functionally associated to PSII, α_{LHII} (m^{-1}), is calculated following Eq. 3 and corrected for the effects of baseline fluorescence, pigment packaging, and spectral differences between MLED and ALED (see also Supporting Information Material S1). JV_{PII} ($\mu\text{mol e}^{-} \text{m}^{-3} \text{s}^{-1}$) is calculated following Eq. 2 and particulate organic carbon (POC) production ($\mu\text{mol C m}^{-3} \text{s}^{-1}$) measured using ^{14}C , as described in the methods. The electron requirement for carbon fixation ($\Phi_{e,c}$, $\text{e}^{-} \text{C}^{-1}$) is derived as $JV_{\text{PII}}/\text{POC}$.

Sample	Local time	$\mu\text{mol photon m}^{-2} \text{s}^{-1}$	nm PSII^{-1}		F_v/F_m	F_q'/F_{mc}'	m^{-1}	$\mu\text{mol e}^{-} \text{m}^{-3} \text{s}^{-1}$	$\mu\text{mol C m}^{-3} \text{s}^{-2}$	$\text{e}^{-} \text{C}^{-1}$
		LL	σ_{PII}	$\sigma_{\text{PII}'}$						
TP1	06:00	30	7.0	5.8	0.43	0.33	0.011	0.08	0.017	4.8
TP2	09:00	30	7.1	5.8	0.43	0.33	0.012	0.09	0.016	5.5
TP3	12:00	30	7.2	6.0	0.34	0.34	0.015	0.08	0.014	5.7
TP4	15:00	30	7.7	6.3	0.35	0.32	0.013	0.11	0.010	10.6
TP5	18:00	30	7.4	6.2	0.38	0.33	0.013	0.10	0.008	12.1
TP6	21:00	30	6.8	5.8	0.40	0.30	0.012	0.07	0.009	7.3
TP2	09:00	20	7.1	6.5	0.43	0.39	0.011	0.07	0.016	4.2
TP3	12:00	330	6.7	3.8	0.32	0.13	0.014	0.29	0.052	5.6
TP4	15:00	300	7.5	4.2	0.33	0.13	0.013	0.25	0.044	5.6
TP5	18:00	100	7.4	5.6	0.38	0.25	0.012	0.18	0.019	9.8

intensity at the time and depth of sampling. These were 30, 330, 300, 100 $\mu\text{mol photon m}^{-2} \text{s}^{-1}$ at 09:00 h, 12:00 h, 15:00 h, 18:00 h, respectively. Both JV_{PII} (Fig. 7D; Table 4) and ^{14}C -fixation (Fig. 7E; Table 4) roughly follow the diurnal cycle in light availability, as expected. However, the decrease in ^{14}C -fixation in the second half of the day is much stronger than the observed decrease in JV_{PII} , resulting in higher value of $\Phi_{e,c}$ in the evening (Fig. 7F; Table 4).

Discussion

In comparison to physical and chemical properties, our ability to measure and monitor biological rates in the ocean is poor, both in terms of accuracy and measurement resolution. This limits our ability to assess how aquatic ecosystems respond to natural variability over a range of time and space scales and may respond to anthropogenic change.

Quantifying photosynthesis and primary productivity is complicated by the fact that photosynthesis is a long chain of diverse, dynamically regulated and partially de-coupled reactions, starting with the absorption of light energy and ending with the “fixation” of inorganic carbon to organic carbon biomass (Blankenship 2008). Furthermore, a proportion of initially fixed carbon (gross carbon fixation) is subsequently respired by phytoplankton, reducing the amount of organic carbon available to higher trophic levels (net carbon fixation). Finally, a non-negligible and variable fraction of fixed carbon can be excreted by live phytoplankton or lost during cell lysis

as DOC (Moran et al. 2022). This fraction is often excluded from estimates of particulate carbon fixation using approaches such as ^{14}C -fixation experiments.

It is thus important to understand at what point a rate is measured along the “metabolic continuum of primary productivity” with a particular method, and which methodological artifacts could lead to misinterpretation of rates. At the same time, careful comparisons of multiple rates of photosynthesis allows for an appreciation of the multiple feedback mechanisms that evolved to optimize function within a fluctuating growth environment. In the context of an overreaching goal to improve our ability to monitor and model changes of phytoplankton primary productivity on a global scale, such mechanistic understanding is arguably as important as accurate and high-resolution in situ data.

In the following we will discuss, in turn, the derivation of JV_{PII} from STAF measurements, the ^{14}C -fixation method for the assessment of phytoplankton primary production in carbon units, and the apparent coupling between the two rates observed using our dual-incubation approach. We conclude with a section on future directions in the application of STAF for the assessment of phytoplankton primary production.

JV_{PII} from STAF

STAF provides estimates of phytoplankton photosynthetic rates at the level of charge separation in PSII (JV_{PII}). Derivation of this rate is not without its caveats, particularly in mixed phytoplankton assemblages in the field. However, advances in

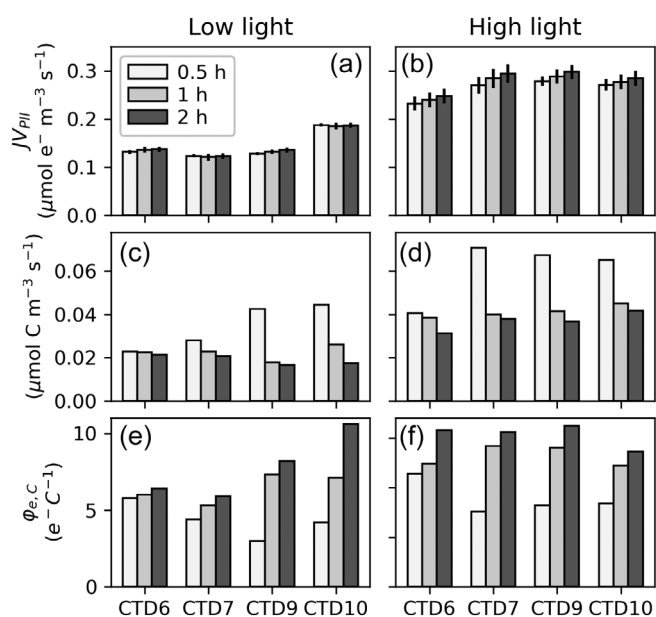


Fig. 5. Dual-incubation time-course experiment (dataset 1). Samples from four stations were used for dual-incubations at light limitation ($50 \mu\text{mol photon m}^{-2} \text{s}^{-1}$, left column) and light saturation ($300 \mu\text{mol photon m}^{-2} \text{s}^{-1}$, right column). During each of the incubations, STAF measurements for JV_{PII} were acquired continuously and averaged over the incubation times (subplots **A** and **B**, error bars are standard deviation). Subsamples were taken at 0.5, 1, and 2 h and processed for analysis of ^{14}C -fixation (subplots **C** and **D**). Subplots **E** and **F** show the derived values of $\Phi_{e,C}$.

both sensor technology and data analysis approaches have significantly improved our ability to acquire intercomparable rates, autonomously and at high resolution (Schuback et al. 2021). In our analysis of primary STAF data, three important correction approaches were applied to improve the estimation of JV_{PII} , which we consider in turn below.

The automated spectral correction approach utilizing photosynthetic excitation profiles (PEP) using the multi-spectral STAF technique described here provides a convenient solution to a problem which has for a long time limited our ability to derive intercomparable and ecologically relevant rates of JV_{PII} (Moore et al. 2006; Szabó et al. 2014; Silsbe et al. 2015; Hughes et al. 2018b; Schuback et al. 2021). PEP data can be acquired fully autonomously and at high resolution. The data can be applied automatically to correct JV_{PII} data to be specific to spectral light distribution within the incubation chamber (as done in this study), but also, importantly, to correct rates of, for example, JV_{PII} or ^{14}C -fixation measured ex situ to derive rates realized at in situ spectral light distribution. As shown in Fig. 3, the value of cPEP derived utilizing the PEP measured by the LabSTAF instrument closely match the spectral correction factors derived using phytoplankton absorption spectra at (0.46 and 0.45, respectively; Fig. 3). While these first results are very promising, it is clear that larger dataset of parallel measurements of PEP and phytoplankton light absorption

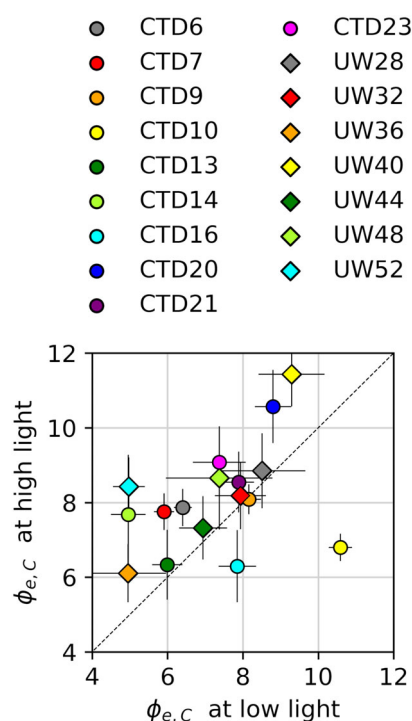


Fig. 6. Two light-level dual-incubation experiments (dataset 2). Samples were collected at 20 m depth from 10 CTD-rosette stations and at 5 m depth from 7 underway (UW) stations. For each sample, 2 h dual-incubations were performed under light-limitating (30 and $50 \mu\text{mol photon m}^{-2} \text{s}^{-1}$ for UW and CTD samples, respectively) and light-saturating (200 and $300 \mu\text{mol photon m}^{-2} \text{s}^{-1}$ for UW and CTD samples, respectively) irradiances. Error bars are the propagated error from duplicate ^{14}C -fixation filtrations for each sample and the standard deviation of JV_{PII} measured throughout the 2 h incubation time.

spectra using approaches such as the filter-pad method, HPLC pigment reconstruction and fluorescence excitation spectra are necessary to further validate the approach.

Observed changes in the PEP across space and time will be driven by changes in phytoplankton community composition (Gorbunov et al. 2020). The present dataset, collected in a geographically constrained region over a relatively short period likely represents relatively limited variation in phytoplankton community compositions, consistent with the observed low variability in cPEP which was also not correlated to any of the measured environmental parameters (Supporting Information Material S3). However, high-resolution PEP data from STAF instruments connected to continuous seawater supplies on board research vessels or deployed on autonomous sampling platforms holds potential to provide a sensitive proxy for changes in phytoplankton community composition in space and time. Furthermore, it is possible to scale the relative values of PEP used for spectral correction to absolute values of absorption coefficients with units of m^{-1} . Such high-resolution in situ measurements of multispectral absorption coefficients specific to pigments functionally associated with

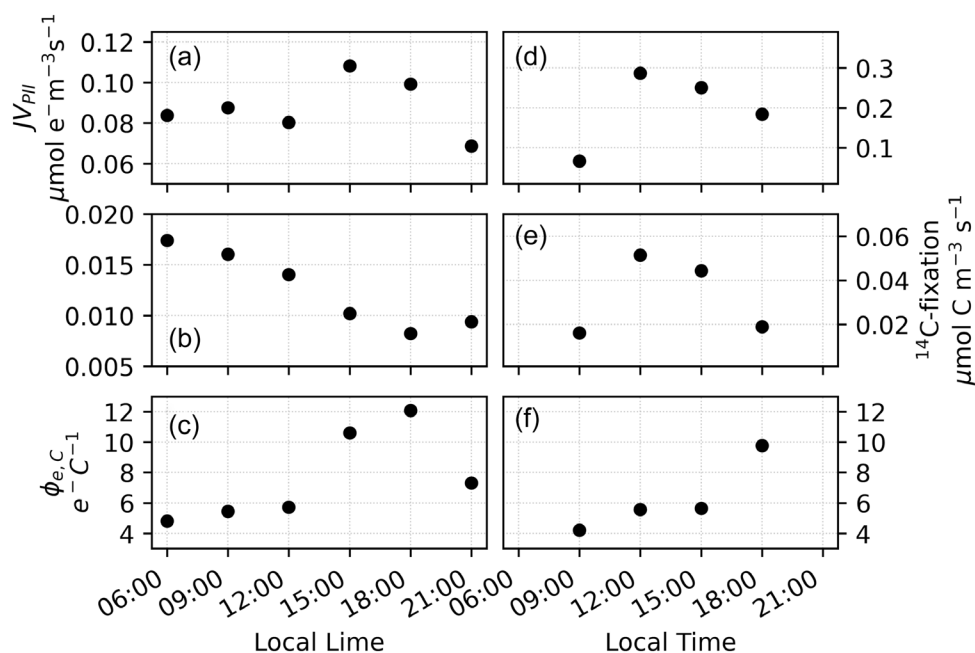


Fig. 7. Diurnal variation in JV_{PII} , ^{14}C -fixation and $\Phi_{e,C}$ (dataset 3). Samples were taken from the continuous seawater supply (5 m depth) at 3 h intervals on 21 March 2022 and incubated at a constant light level of $30 \mu\text{mol photon m}^{-2} \text{s}^{-1}$ for each time-point (left column) or at an estimated in situ light intensity at time and depth of sampling (right column). Incubation time was 2 h.

PSII (a_{LHII}) and maximum photosynthetic light utilization by PSII (a_{PII}) could be of great value for the parameterization of absorption-based models of phytoplankton primary productivity.

Dual-waveband measurements (DWM) of fluorescence emission at 680 and 730 nm can be utilized to estimate the relative fraction of ST fluorescence signal at 680 nm reabsorbed by Chl *a* (Boatman et al. 2019; Oxborough 2022; Fig. 3). From these measurements, a correction factor (cPEC) is derived. Despite the limited range of environmental conditions encountered in the present dataset, a correlation of DWM and [Chl *a*] ($r^2 = 0.65$, $n = 60$; Supporting Information material S3) was observed, as would be expected for a proxy of pigment packaging (Woźniak et al. 1999; Le et al. 2009; Letelier et al. 2017). However, as the approach has only been implemented recently it clearly requires further validation against independent measurements, both in the field and under controlled laboratory conditions. If future work confirms the validity of the approach for high-resolution, autonomous collection of pigment packaging estimates, data will not only improve our ability to calculate JV_{PII} but would also be very useful in, for example, the interpretation of solar induced fluorescence (Babin et al. 1996; Huot et al. 2005; Gupana et al. 2021).

Baseline fluorescence, the non-variable fluorescence signal emanating predominantly from Chl *a* not functionally associated with PSII, is a well-recognized problem for the accurate derivation of photosynthetic rates from STAF data. Similar to non-inducible fluorescence from the medium surrounding phytoplankton (the “blank”, see e.g., Cullen and Davis 2003),

baseline fluorescence increases minimum (F_o or F') and maximum (F_m or F_m') fluorescence to the same extent, leading to a reduction in the derived values for F_v/F_m or F_q'/F_m' . Increases in baseline fluorescence caused by Chl *a* in so-called energetically disconnected light harvesting complexes therefore provides a sensitive and useful diagnostic of iron limitation (Behrenfeld and Milligan 2013). However, it is problematic for the calculation of JV_{PII} from STAF data. All approaches for the calculation of JV_{PII} are based on the concept of three complementary pathways of energy dissipation within PSII: absorbed light energy is distributed between fluorescence, heat dissipation, and photochemistry (Butler 1978). Because these three pathways are complementary, changes in heat dissipation and photochemistry modulate fluorescence and observed changes in fluorescence can be interpreted in terms of photochemistry. However, the models used to interpret changes in fluorescence based on this concept only strictly apply if all detected fluorescence originates from sources where the three pathways are indeed available, which is not the case for baseline fluorescence.

As baseline fluorescence can be caused by a multitude of factors (e.g., energetically disconnected light harvesting complexes, photoinhibition, PSI fluorescence, etc.), there is no simple method for correction (Schuback et al. 2021). Based on laboratory experiments, Boatman et al. (2019) suggested correcting all measurements with a measured value of F_v/F_m below an “intrinsic” value of 0.54, that is, an assumed maximum PSII photochemical yield, for baseline fluorescence (F_b ; Eqs. 5, 6). In the present field study, we applied an

“inherent” F_v/F_{mc} value of 0.5 and provide an analysis of the effect of different F_v/F_{mc} in Supporting Information Material S2. We do not claim that the baseline fluorescence correction applied in this study is the best and universally applicable approach. However, it likely represents the best solution at present to a well-recognized problem. Clearly, more work is needed to better understand sources of, and corrections for, baseline fluorescence, in particular under contrasting environmental conditions including iron limitation.

In conclusion, improved measurement capabilities of LabSTAF instruments allow for automated acquisition of a range of parameters which allow for improved estimates of photosynthetic rates as JV_{PII} . As in particular PEP and DWM data have considerable potential in their own right, we encourage the LabSTAF user community to deposit raw and meta data in openly accessible repositories such as this collection set up in Zenodo (https://zenodo.org/communities/staf_underway). Collectively, intercomparable global datasets will be invaluable for further validation of the measurements, allow observation of environmentally driven patterns in phytoplankton optical properties in space and time, and provide input for the development of models and remote sensing algorithms.

¹⁴C-fixation

Despite its many well recognized limitations, ¹⁴C-fixation is considered the gold-standard of phytoplankton primary productivity measurements (IOCCG 2022). The results presented in this study illustrate several aspects of the ¹⁴C-fixation approach which complicate the use of this method for the collection of consistent datasets, fundamental for development and validation of numerical modeling and remote sensing approaches.

The time-course experiments which show systematic declines in derived rates over 0.5–2 h timescales (Fig. 4), demonstrate that 2 h long incubations likely do not yield rates of gross primary production, as frequently assumed in the literature (e.g., Brewin et al. 2023). Importantly, work by Halsey et al. (2011, 2013) and Pei and Laws (2013) has shown that standardized incubation lengths for ¹⁴C-fixation experiments will estimate rates at different points along the gross-to-net carbon fixation continuum, depending on environmental conditions, because nutrient-limited, slow-growing phytoplankton will tend to respire initially fixed ¹⁴C faster than nutrient-replete, fast-growing cells. Thus, global datasets of 2 h long ¹⁴C-fixation experiments could introduce systematic error, tending to underestimate gross primary productivity in regions where phytoplankton growth is limited by the availability of nutrients compared to more nutrient replete regions.

The diurnal experiment (Fig. 7) illustrates that carbon fixation, as measured with 2 h ¹⁴C-fixation experiments, is highest at dawn and decreases throughout the day. This is consistent with previous studies (Bruyant et al. 2005; Schuback et al. 2016; Schuback and Tortell 2019) and can be

explained by metabolic shifts in cellular energy allocation, potentially amplified further depending on where on the gross-to-net carbon fixation continuum the rate is estimated by the 2 h incubations, if diurnal changes in respiration occur. Diurnal variability in rates of primary productivity as measured by short-term ¹⁴C-fixation experiments can be large and amplified under nutrient limitation (Schuback and Tortell 2019), leading to further inconsistencies in global data compilations. Finally, if the experimental approach includes filtration of the ¹⁴C-labeled sample, a significant and variable amount of initially fixed ¹⁴C will inevitably be lost as DOC, introducing further errors in the estimation of net primary productivity, defined as the formation of organic matter from inorganic compounds minus the respiratory losses of photosynthetic organisms.

In our experiments, “dark” correction led to a significant reduction in calculated rates of ¹⁴C-fixation (mean = 15%, range = 4–53%). Time zero samples, where a sample was spiked and immediately filtered were done on three occasions and with 45 ± 11 DPM mL⁻¹ statistically not different than the 47 ± 16 DPM mL⁻¹ of DPM_{dark}. This indicates that the DPM measured after incubation in the dark are not metabolic fixation of inorganic ¹⁴C, but rather a background of inorganic ¹⁴C bound to the GFF filter and not removed by the acidification step. The dual-incubation experiments require small incubation volumes and short incubation times. In particular under low biomass conditions, this necessitates a high ¹⁴C spike (1 μCi mL⁻¹), leading to high background DPM. Correction for this background signal is crucial and we recommend that both, time zero and dark incubations, are performed alongside each dual-incubation experiment to minimize the possible error introduced to estimates of ¹⁴C-fixation.

In conclusion, we emphasize that interpretation of $\Phi_{e,C}$ values from dual-incubation experiments requires consideration of caveats for both, the estimation of JV_{PII} from STAF and the rate of carbon fixation from ¹⁴C-fixation experiments.

Electron to carbon ratio, $\Phi_{e,C}$

In our dataset, derived values of $\Phi_{e,C}$ ranged from 3.0 to 12.1 e⁻ C⁻¹ with a mean value of 7.0 e⁻ C⁻¹ ($n = 60$; Tables 2–4). Thus, values are mostly above the theoretical minimum of 4 e⁻ C⁻¹, and within a narrower range than what has been previously observed (Lawrenz et al. 2013; Hughes et al. 2018b). The narrow range of values can be partially explained by the limited geographical and temporal range of sampling, where nutrient levels remained above levels considered limiting for growth (Table 1). This is further confirmed by the absence of any correlation of $\Phi_{e,C}$ with either nutrient concentrations (Lawrenz et al. 2013; Hughes et al. 2018a) or measured levels of non-photochemical quenching (Schuback et al. 2015; Hughes et al. 2020), although some of the observed variability in $\Phi_{e,C}$ could be related to known physiological mechanisms. Larger datasets of dual-incubation experiments, under a range of environmental conditions, will be

required to fully characterize the magnitude and variability of $\Phi_{e,C}$ estimated in this manner in the oceans. However, removing a number of methodological biases which significantly limited previous intercomparisons of the two techniques is an important step toward the goal of understanding the true variability in electron to carbon ratios and their environmental drivers.

Future directions and recommendations

Arguably, the greatest advantage of optical measurements such as STAF is automated, high-resolution acquisition of methodologically consistent data. Completely autonomous deployments of STAF on platforms like moorings, floats and gliders is now feasible, with obvious potential to improve spatial and temporal coverage of phytoplankton photophysiology and photosynthetic rate estimates. Completely automated data acquisition is also possible for light-response curves, where rates of photosynthesis, estimated as JV_{PII} , are derived under a range of background irradiances. Akin to ^{14}C photosynthesis–irradiance (P–E) curves, this allows the derivation of the fit parameter α , P_{max} , and E_k —corresponding respectively to the initial slope, the light saturated maximum value and the saturation light intensity of the photosynthesis–irradiance response (Sakshaug et al. 1997). Global compilations of these parameters (Bouman et al. 2018; Kulk et al. 2020) are to date one of the most common inputs for the parameterization of the photosynthetic efficiency in remote sensing algorithms of phytoplankton primary production (Friedrichs et al. 2009; Saba et al. 2011; Lee et al. 2015b; Westberry et al. 2023). The strong sensitivity of such algorithms to P–E curve parameters was demonstrated by Kulk et al. (2020), who showed that changing P–E parameters from a global compilation by one standard deviation resulted in 45–47% change in derived primary productivity. Considering the many uncertainties inherent to ^{14}C -fixation experiments discussed above, such results indicate that complete reliance on compilations of just this one methodological approach may introduce biases, suggesting that other techniques be explored.

With this in mind, we stress that it is not our aim to “calibrate” STAF derived JV_{PII} against ^{14}C -fixation, as the use of this method as a gold-standard is clearly questionable. Rather, we support the proposal of Hughes et al. (2018b), who argue that JV_{PII} should be better appreciated as a fundamental biological rate, which defines the overall amount of light energy and associated reduction potential is entering an ecosystem and therefore reflects a fundamental constraint to its function. How this input of energy and reductant can subsequently be partitioned within the primary producers and the wider ecosystem, including how much is used for gross carbon fixation, how much fixed carbon is respired by photosynthetic and heterotrophic organisms, how much carbon is ultimately exported by the “biological pump,” and how these processes are controlled by environmental drivers are crucial questions

which, in turn, need to be addressed. Large datasets of $\Phi_{e,C}$ from the dual-incubation approach presented here, if interpreted with care, are one way to improve our understanding of how ecosystem metabolisms dynamically react and adjust to environmental change. Looking forward, studies comparing STAF-derived JV_{PII} with the many other approaches available to quantify phytoplankton primary productivity over a range of space and time, will be of particular importance.

Data availability statement

Schuback, N. (2024). Data for: Phytoplankton primary productivity: a dual-incubation approach for direct comparison of photosystem II photosynthetic flux (JV_{PII}) and ^{14}C -fixation experiments [Data set]. Zenodo. <https://doi.org/10.5281/zenodo.10809209>.

References

- Babin, M., A. Morel, and B. Gentili. 1996. Remote sensing of sea surface sun-induced chlorophyll fluorescence: Consequences of natural variations in the optical characteristics of phytoplankton and the quantum yield of chlorophyll *a* fluorescence. *Int. J. Remote Sens.* **17**: 2417–2448. doi:10.1080/01431169608948781
- Bax, N. J., and others. 2019. A response to scientific and societal needs for marine biological observations. *Front. Mar. Sci.* **6**: 395. doi:10.3389/FMARS.2019.00395
- Becker, S., and others. 2020. GO-SHIP repeat hydrography nutrient manual: The precise and accurate determination of dissolved inorganic nutrients in seawater, using continuous flow analysis methods. *Front. Mar. Sci.* **7**: 581790. doi:10.3389/fmars.2020.581790
- Behrenfeld, M. J., and P. G. Falkowski. 1997. Photosynthetic rates derived from satellite-based chlorophyll concentration. *Limnol. Oceanogr.* **42**: 1–20. doi:10.4319/LO.1997.42.1.0001
- Behrenfeld, M. J., and A. J. Milligan. 2013. Photophysiological expressions of iron stress in phytoplankton. *Ann. Rev. Mar. Sci.* **5**: 217–246. doi:10.1146/annurev-marine-121211-172356
- Behrenfeld, M. J., K. H. Halsey, and A. J. Milligan. 2008. Evolved physiological responses of phytoplankton to their integrated growth environment. *Philos. Trans. R. Soc. Lond. B Biol. Sci.* **363**: 2687–2703. doi:10.1098/rstb.2008.0019
- Behrenfeld, M. J., and others. 2006. Climate-driven trends in contemporary ocean productivity. *Nature* **444**: 752–755. doi:10.1038/nature05317
- Blankenship, R. E. [ed.]. 2008. Molecular mechanisms of photosynthesis. Wiley-Blackwell.
- Boatman, T. G., R. J. Geider, and K. Oxborough. 2019. Improving the accuracy of single turnover active fluorometry (STAF) for the estimation of phytoplankton primary

- productivity (PhytoPP). *Front. Mar. Sci.* **6**: 319. doi:10.3389/fmars.2019.00319
- Bouman, H. A., T. Jackson, S. Sathyendranath, and T. Platt. 2020. Vertical structure in chlorophyll profiles: Influence on primary production in the Arctic Ocean. *Philos. Trans. A. Math. Phys. Eng. Sci.* **378**: 20190351. doi:10.1098/rsta.2019.0351
- Bouman, H. A., and others. 2018. Photosynthesis-irradiance parameters of marine phytoplankton: Synthesis of a global data set. *Earth Syst. Sci. Data* **10**: 251–266. doi:10.5194/essd-10-251-2018
- Brewin, R. J. W., and others. 2023. Ocean carbon from space: Current status and priorities for the next decade. *Earth-Sci. Rev.* **240**: 104386. doi:10.1016/j.earscirev.2023.104386
- Bruyant, F., and others. 2005. Diel variations in the photosynthetic parameters of *Prochlorococcus* strain PCC 9511: Combined effects of light and cell cycle. *Limnol. Oceanogr.* **50**: 850–863. doi:10.4319/lo.2005.50.3.0850
- Butler, W. L. 1978. Energy distribution in the photochemical apparatus of photosynthesis. *Annu. Rev. Plant Biol.* **29**: 345–378. doi:10.1146/annurev.pp.29.060178.002021
- Call, M., K. G. Schultz, M. C. Carvalho, I. R. Santos, and D. T. Maher. 2017. Technical note: Coupling infrared gas analysis and cavity ring down spectroscopy for autonomous, high-temporal-resolution measurements of DIC and $\delta^{13}\text{C}$ -DIC. *Biogeosciences* **14**: 1305–1313. doi:10.5194/bg-14-1305-2017
- Ciotti, Á. M., M. R. Lewis, and J. J. Cullen. 2002. Assessment of the relationships between dominant cell size in natural phytoplankton communities and the spectral shape of the absorption coefficient. *Limnol. Oceanogr.* **47**: 404–417. doi:10.4319/lo.2002.47.2.0404
- Corno, G., R. M. Letelier, M. R. Abbott, and D. M. Karl. 2006. Assessing primary production variability in the North Pacific Subtropical Gyre: A comparison of fast repetition rate fluorometry and ^{14}C measurements. *J. Phycol.* **42**: 51–60. doi:10.1111/j.1529-8817.2006.00163.x
- Cullen, J. J., and R. F. Davis. 2003. The blank can make a big difference in oceanographic measurements. *Limnol. Oceanogr.: Bull.* **12**: 29–35. doi:10.1007/s00360-007-0169-0
- Doney, S. C., and others. 2012. Climate change impacts on marine ecosystems. *Ann. Rev. Mar. Sci.* **4**: 11–37. doi:10.1146/annurev-marine-041911-111611
- Friedrichs, M. A. M., and others. 2009. Assessing the uncertainties of model estimates of primary productivity in the tropical Pacific Ocean. *J. Mar. Syst.* **76**: 113–133. doi:10.1016/j.jmarsys.2008.05.010
- Fujiki, T., T. Suzue, H. Kimoto, and T. Saino. 2007. Photosynthetic electron transport in *Dunaliella tertiolecta* (Chlorophyceae) measured by fast repetition rate fluorometry: Relation to carbon assimilation. *J. Plankton Res.* **29**: 199–208. doi:10.1093/plankt/fbm007
- Genty, B., J. M. Briantais, and N. R. Baker. 1989. The relationship between the quantum yield of photosynthetic electron transport and quenching of chlorophyll fluorescence. *Biochim. Biophys. Acta Gen. Subj.* **990**: 87–92. doi:10.1016/S0304-4165(89)80016-9
- Gorbunov, M. Y., E. Shirsin, E. Nikonova, V. V. Fadeev, and P. G. Falkowski. 2020. A multi-spectral fluorescence induction and relaxation (fire) technique for physiological and taxonomic analysis of phytoplankton communities. *Mar. Ecol. Prog. Ser.* **644**: 1–13. doi:10.3354/meps13358
- Greene, R. M., Z. S. Kolber, D. G. Swift, N. W. Tindale, and P. G. Falkowski. 1994. Physiological limitation of phytoplankton photosynthesis in the eastern equatorial Pacific determined from variability in the quantum yield of fluorescence. *Limnol. Oceanogr.* **39**: 1061–1074. doi:10.4319/lo.1994.39.5.1061
- Gupana, R. S., D. Odermatt, I. Cesana, C. Giardino, L. Nedbal, and A. Damm. 2021. Remote sensing of sun-induced chlorophyll-*a* fluorescence in inland and coastal waters: Current state and future prospects. *Remote Sens. Environ.* **262**: 112482. doi:10.1016/j.rse.2021.112482
- Halsey, K. H., A. J. Milligan, and M. J. Behrenfeld. 2011. Linking time-dependent carbon-fixation efficiencies in *Dunaliella tertiolecta* (Chlorophyceae) to underlying metabolic pathways. *J. Phycol.* **47**: 66–76. doi:10.1111/j.1529-8817.2010.00945.x
- Halsey, K. H., R. T. O'Malley, J. R. Graff, A. J. Milligan, and M. J. Behrenfeld. 2013. A common partitioning strategy for photosynthetic products in evolutionarily distinct phytoplankton species. *New Phytol.* **198**: 1030–1038. doi:10.1111/nph.12209
- Halsey, K. H., and B. M. Jones. 2015. Phytoplankton strategies for photosynthetic energy allocation. *Ann. Rev. Mar. Sci.* **7**: 265–297. doi:10.1146/annurev-marine-010814-015813
- Hughes, D. J., D. Varkey, M. A. Doblin, T. Ingleton, A. McInnes, P. J. Ralph, V. van Dongen-Vogels, and D. J. Suggett. 2018a. Impact of nitrogen availability upon the electron requirement for carbon fixation in Australian coastal phytoplankton communities. *Limnol. Oceanogr.* **63**: 1891–1910. doi:10.1002/lno.10814
- Hughes, D. J., J. R. Crosswell, M. A. Doblin, K. Oxborough, P. J. Ralph, D. Varkey, and D. J. Suggett. 2020. Dynamic variability of the phytoplankton electron requirement for carbon fixation in eastern Australian waters. *J. Mar. Syst.* **202**: 103252. doi:10.1016/j.jmarsys.2019.103252
- Hughes, D. J., F. C. Giannini, A. M. Ciotti, M. A. Doblin, P. J. Ralph, D. Varkey, A. Verma, and D. J. Suggett. 2021. Taxonomic variability in the electron requirement for carbon fixation across marine phytoplankton. *J. Phycol.* **57**: 111–127. doi:10.1111/jpy.13068
- Hughes, D. J., and others. 2018b. Roadmaps and detours: Active chlorophyll-*a* assessments of primary productivity across marine and freshwater systems. *Environ. Sci. Technol.* **52**: 12039–12054. doi:10.1021/acs.est.8b03488
- Huot, Y., C. A. Brown, and J. J. Cullen. 2005. New algorithms for MODIS sun-induced chlorophyll fluorescence and a

- comparison with present data products. *Limnol. Oceanogr.: Methods* **3**: 108–130. doi:10.4319/lom.2005.3.108
- Intergovernmental Panel on Climate Change (IPCC). 2019. *In* H.-O. Pörtner and others [eds.], IPCC special report on the ocean and cryosphere in a changing climate. Cambridge University Press. doi:10.1017/9781009157964
- International Ocean-Colour Coordinating Group (IOCCG). 2022. Aquatic primary productivity field protocols for satellite validation and model synthesis. *In* R. A. Vandermeulen and J. E. Chaves [eds.], Ocean optics and biogeochemistry protocols for Satellite Ocean colour sensor validation. IOCCG. doi:10.25607/OBP-1835
- Kolber, Z., and P. G. Falkowski. 1993. Use of active fluorescence to estimate phytoplankton photosynthesis in situ. *Limnol. Oceanogr.* **38**: 1646–1665. doi:10.4319/lo.1993.38.8.1646
- Kulk, G., and others. 2020. Primary production, an index of climate change in the ocean: Satellite-based estimates over two decades. *Remote Sens.* **12**: 826. doi:10.3390/rs12050826
- Lawrenz, E., and others. 2013. Predicting the electron requirement for carbon fixation in seas and oceans. *PLoS One* **8**: e58137. doi:10.1371/journal.pone.0058137
- Le, C., Y. Li, Y. Zha, and D. Sun. 2009. Specific absorption coefficient and the phytoplankton package effect in Lake Taihu, China. *Hydrobiologia* **619**: 27–37. doi:10.1007/s10750-008-9579-6
- Lee, Z., J. Marra, M. J. Perry, and M. Kahru. 2015a. Estimating oceanic primary productivity from ocean color remote sensing: A strategic assessment. *J. Mar. Syst.* **149**: 50–59. doi:10.1016/j.jmarsys.2014.11.015
- Lee, Y. J., and others. 2015b. An assessment of phytoplankton primary productivity in the Arctic Ocean from satellite ocean color/in situ chlorophyll-*a* based models. *J. Geophys. Res.: Oceans* **120**: 6508–6541. doi:10.1002/2015JC011018
- Letelier, R. M., A. E. White, R. R. Bidigare, B. Barone, M. J. Church, and D. M. Karl. 2017. Light absorption by phytoplankton in the North Pacific Subtropical Gyre. *Limnol. Oceanogr.* **62**: 1526–1540. doi:10.1002/lno.10515
- Li, Z., W. Yang, B. Matsushita, and A. Kondoh. 2022. Remote estimation of phytoplankton primary production in clear to turbid waters by integrating a semi-analytical model with a machine learning algorithm. *Remote Sens. Environ.* **275**: 113027. doi:10.1016/J.RSE.2022.113027
- Lombard, F., and others. 2019. Globally consistent quantitative observations of planktonic ecosystems. *Front. Mar. Sci.* **6**: 196. doi:10.3389/fmars.2019.00196
- Milligan, A. J., K. H. Halsey, and M. J. Behrenfeld. 2014. HORIZONS: Advancing interpretations of ¹⁴C-uptake measurements in the context of phytoplankton physiology and ecology. *J. Plankton Res.* **37**: 692–698. doi:10.1093/plankt/fbv051
- Moore, C. M., D. J. Suggett, A. E. Hickman, Y. N. Kim, J. F. Tweddle, J. Sharples, R. J. Geider, and P. M. Holligan. 2006. Phytoplankton photoacclimation and photoadaptation in response to environmental gradients in a shelf sea. *Limnol. Oceanogr.* **51**: 936–949. doi:10.4319/lo.2006.51.2.0936
- Moran, M. A., and others. 2022. The Ocean's labile DOC supply chain. *Limnol. Oceanogr.* **67**: 1007–1021. doi:10.1002/lno.12053
- Oxborough, K. 2022. LabSTAF and RunSTAF Handbook: 2408-014-HB | Issue F. West Molesey, UK, Chelsea Technologies Ltd. 171pp. (Doc No. 2408-014-HB | Issue F). doi:10.25607/OBP-1029.4
- Oxborough, K., C. M. Moore, D. J. Suggett, T. Lawson, H. G. Chan, and R. J. Geider. 2012. Direct estimation of functional PSII reaction center concentration and PSII electron flux on a volume basis: A new approach to the analysis of fast repetition rate fluorometry (FRRF) data. *Limnol. Oceanogr.: Methods* **10**: 142–154. doi:10.4319/lom.2012.10.142
- Pedrés, R., I. Moya, Y. Goulas, and S. Jacquemoud. 2008. Chlorophyll fluorescence emission spectrum inside a leaf. *Photochem. Photobiol. Sci.* **7**: 498–502. doi:10.1039/b719506k
- Pei, S., and E. A. Laws. 2013. Does the ¹⁴C method estimate net photosynthesis? Implications from batch and continuous culture studies of marine phytoplankton. *Deep-Sea Res. I: Oceanogr. Res. Pap.* **82**: 1–9. doi:10.1016/j.dsr.2013.07.011
- Peterson, B. J. 1980. Aquatic primary productivity and the ¹⁴C-CO₂ method: A history of the productivity problem. *Annu. Rev. Ecol. Syst.* **11**: 359–385. doi:10.1146/annurev.es.11.110180.002043
- Saba, V. S., and others. 2011. An evaluation of ocean color model estimates of marine primary productivity in coastal and pelagic regions across the globe. *Biogeosciences* **8**: 489–503. doi:10.5194/bg-8-489-2011
- Sakshaug, E., and others. 1997. Parameters of photosynthesis: Definitions, theory and interpretation of results. *J. Plankton Res.* **19**: 1637–1670. doi:10.1093/plankt/19.11.1637
- Schuback, N., C. Schallenberg, C. Duckham, M. T. Maldonado, and P. D. Tortell. 2015. Interacting effects of light and iron availability on the coupling of photosynthetic electron transport and CO₂-assimilation in marine phytoplankton. *PLoS One* **10**: e0133235. doi:10.1371/journal.pone.0133235
- Schuback, N., M. Flecken, M. T. Maldonado, and P. D. Tortell. 2016. Diurnal variation in the coupling of photosynthetic electron transport and carbon fixation in iron-limited phytoplankton in the NE subarctic Pacific. *Biogeosciences* **13**: 1019–1035. doi:10.5194/bg-13-1019-2016
- Schuback, N., C. J. M. Hoppe, J.-É. Tremblay, M. T. Maldonado, and P. D. Tortell. 2017. Primary productivity and the coupling of photosynthetic electron transport and carbon fixation in the Arctic Ocean. *Limnol. Oceanogr.* **62**: 898–921. doi:10.1002/lno.10475
- Schuback, N., and P. D. Tortell. 2019. Diurnal regulation of photosynthetic light absorption, electron transport and

- carbon fixation in two contrasting oceanic environments. *Biogeosciences* **16**: 1381–1399. doi:10.5194/bg-16-1381-2019
- Schuback, N., and others. 2021. Single-turnover variable chlorophyll fluorescence as a tool for assessing phytoplankton photosynthesis and primary productivity: Opportunities, caveats and recommendations. *Front. Mar. Sci.* **8**: 690607. doi:10.3389/fmars.2021.690607
- Silsbe, G. M., and others. 2015. Toward autonomous measurements of photosynthetic electron transport rates: An evaluation of active fluorescence-based measurements of photochemistry. *Limnol. Oceanogr.: Methods* **13**: 138–155. doi:10.1002/lom3.10014
- Stemann-Nielsen, E. 1952. The use of radio-active carbon (C^{14}) for measuring organic production in the sea. *ICES J. Mar. Sci.* **18**: 117–140. doi:10.1093/icesjms/18.2.117
- Suggett, D. J., H. L. MacIntyre, T. M. Kana, and R. J. Geider. 2009. Comparing electron transport with gas exchange: Parameterising exchange rates between alternative photosynthetic currencies for eukaryotic phytoplankton. *Aquat. Microb. Ecol.* **56**: 147–162. doi:10.3354/ame01303
- Szabó, M., and others. 2014. Photosynthetic acclimation of *Nannochloropsis oculata* investigated by multi-wavelength chlorophyll fluorescence analysis. *Bioresour. Technol.* **167**: 521–529. doi:10.1016/j.biortech.2014.06.046
- Tortell, P. D., N. Schuback, and D. J. Suggett. 2023. Application of single turnover active chlorophyll fluorescence for phytoplankton productivity measurements. Version 2.0. SCOR Working Group 156. doi:10.25607/OBP-1084
- Viviani, D. A., D. M. Karl, and M. J. Church. 2015. Variability in photosynthetic production of dissolved and particulate organic carbon in the North Pacific Subtropical Gyre. *Front. Mar. Sci.* **2**: 73. doi:10.3389/fmars.2015.00073
- Welschmeyer, N. A. 1994. Fluorometric analysis of chlorophyll *a* in the presence of chlorophyll *b* and pheopigments. *Limnol. Oceanogr.* **39**: 1985–1992. doi:10.4319/lo.1994.39.8.1985
- Westberry, T. K., G. M. Silsbe, and M. J. Behrenfeld. 2023. Gross and net primary production in the global ocean: An ocean color remote sensing perspective. *Earth-Sci. Rev.* **237**: 104322. doi:10.1016/j.earscirev.2023.104322
- Williams, P. J. B., and J. E. Robertson. 1991. Overall planktonic oxygen and carbon dioxide metabolisms: The problem of reconciling observations and calculations of photosynthetic quotients. *J. Plankton Res.* **13**: 153–169. doi:10.1093/oxfordjournals.plankt.a04236
- Williams, P. J. B., D. N. Thomas, and C. S. Reynolds [eds.]. 2002. *Phytoplankton productivity: Carbon assimilation in marine and freshwater ecosystems*. Wiley-Blackwell.
- Woźniak, B., J. Dera, D. Ficek, R. Majchrowski, S. Kaczmarek, M. Ostrowska, and O. I. Koblentz-Mishke. 1999. Modelling the influence of acclimation on the absorption properties of marine phytoplankton. *Oceanologia* **41**: 187–210.
- Zhu, Y., J. Ishizaka, S. C. Tripathy, S. Wang, C. Sukigara, J. Goes, T. Matsuno, and D. J. Suggett. 2017. Relationship between light, community composition and the electron requirement for carbon fixation in natural phytoplankton. *Mar. Ecol. Prog. Ser.* **580**: 83–100. doi:10.3354/meps12310

Acknowledgment

The authors would like to thank the captain and crew of the RRS Discovery during DY149 and all scientists participating in the voyage, in particular Jacob Harper and Neil Wyatt. We would like to acknowledge Efstathios Papadimitriou for the analysis of DIC samples and Ilana Berman-Frank for providing comments on an earlier version of the manuscript. CMM was supported through NERC grant NE/P020844/1. EH and EP acknowledge funding through NERC grant NE/P02081X/1 (CarCASS project). PLG and MDP received funds from the project AutoNutS: Autonomous vehicle Nutrient Sensors (NE/P020798/1) which is part of the NERC Oceanids Programme funded by UK Government through the Industrial Strategy Challenge Fund (ISCF). NS acknowledges the Swiss Polar Institute for facilitating flexible work schedules, Swiss National Railway for keeping their fold-out tables on which the entire manuscript was written, and coffee.

Submitted 14 March 2024

Revised 21 May 2024

Accepted 17 June 2024

Associate editor: Tammi Richardson